VISIBLE WAVELENGTH INTERFEROMETER FOR HIGH SPEED ELECTRON DENSITY DIAGNOSTICS

D. Reilly

Final Technical Report

June 1984

sponsored by

DEFENSE ADVANCED RESEARCH PROJECTS AGENCY
Washington, D.C.

monitored by

NAVAL SERVICE WEAPONS CENTER
White Oak
Silver Spring, MD

UNCLASSIFIED

SECURITY CLASSIFICATION OF THIS PAGE (When Data Entered)

REPORT DOCUMENTATION PAGE	READ INSTRUCTIONS BEFORE COMPLETING FORM
1. REPORT NUMBER	2. GOVT ACCESSION NO. A145686 — 3. RECIPIENT'S CATALOG NUMBER
4. TITLE (and Subtitle) VISIBLE WAVELENGTH INTERFEROMETER FOR HIGH SPEED ELECTRON DENSITY DIAGNOSTICS	5. TYPE OF REPORT & PERIOD COVERED Final Technical Report
	6. PERFORMING ORG. REPORT NUMBER
7. AUTHOR(s) D. Reilly	8. CONTRACT OR GRANT NUMBER(s) N60921-82-C-0141
9. PERFORMING ORGANIZATION NAME AND ADDRESS Avco Everett Research Laboratory, Inc. 2385 Revere Beach Parkway Everett, MA 02149	10. PROGRAM ELEMENT, PROJECT, TASK AREA & WORK UNIT NUMBERS
11. CONTROLLING OFFICE NAME AND ADDRESS Defense Advanced Research Projects Agency Washington, DC	12. REPORT DATE June 1984 — 13. NUMBER OF PAGES
14. MONITORING AGENCY NAME & ADDRESS(if different from Controlling Office) Naval Service Weapons Center White Oak Silver Spring, MD	15. SECURITY CLASS. (of this report) Unclassified — 15a. DECLASSIFICATION/DOWNGRADING SCHEDULE
16. DISTRIBUTION STATEMENT (of this Report)	
17. DISTRIBUTION STATEMENT (of the abstract entered in Block 20, if different from Report)	
18. SUPPLEMENTARY NOTES	
19. KEY WORDS (Continue on reverse side if necessary and identify by block number) Interferometry, Electron Density Measurement, E-Beam Diagnostic	

20. ABSTRACT (Continue on reverse side if necessary and identify by block number)

A high-speed interferometer for measuring line integrated electron-densities produced by the ETA and ATA charged particle beams has been constructed and tested. The device is configured such that only passive, radiation resistant components are in the measurement area, while the active components -- detectors, electronics, and cw visible wavelength laser -- are remotely grouped within a portable screened enclosure. Scene and reference beam beams communicate between the two areas over a common optical path, insensitive to atmospheric distortions. Active feedback maintains system balance. A differential

DD FORM 1 JAN 73 1473 EDITION OF 1 NOV 65 IS OBSOLETE

SECURITY CLASSIFICATION OF THIS PAGE (When Data Entered)

(20)

detection scheme is sensitive to phase information only, reducing photon shot noise and other sources of amplitude modulation.

Measurements were carried out at atmospheric pressure in air, N_2, and Ar using a 3 ns, 6 kA pulse from a Febetron, and in air and Ne over a range of pressures using a 25 ns, 8 kA pulse from the ETA. The system response time of 1.5 ns was sufficient to resolve all of the observed electron density features. The lower detection limit, $\lambda/2\times10^4$, was set by preamplifier noise. This was equivalent to a line integrated RMS electron density uncertainty of 1.3×10^{13} electrons/cm^2. Peak densities, observed in argon, were 1.3×10^{16}/cm^2. Short pulse data agreed with theoretical prediction. Unstable beam propagation in the ETA was characterized by sharp runups of electron-density within the body of a pulse.

TABLE OF CONTENTS

Section		Page
	List of Illustrations	iv
1.0	INTRODUCTION	1
2.0	DEVICE DESCRIPTION	3
	2.1 Control Room I	3
	2.1.1 Mechanical	3
	2.1.2 Laser	6
	2.1.3 Electro-Optic Modulator	6
	2.1.4 Beam Transport	8
	2.2 Optical Strongback	9
	2.2.1 Mechanical Design	9
	2.2.2 Optical Design	13
	2.3 Control Room II	14
	2.3.1 Mixing	15
	2.3.2 Detection	15
	2.3.3 Control Electronics	17
3.0	SYSTEM SETUP	20
	3.1 Electro Mechanical	20
	3.1.1 Power and Water	20
	3.1.2 Screen Room	20
	3.1.3 Strongback	22
	3.2 Optical	22
	3.2.1 Laser Turn On	22
	3.2.2 Modulator Alignment	23
	3.2.3 Optical Train	23

Section			Page
4.0	SYSTEM OPERATION		26
	4.1	Balance Procedure	26
	4.2	Calibration	28
	4.3	Power Levels and Sensitivity	32
		4.3.1 Laser Power	32
		4.3.2 Transmission Factors	32
		4.3.3 Detector Response	35
		4.3.4 Fringe Contrast	35
		4.3.5 Detector Response Time	36
5.0	EXPERIMENTAL RESULTS		40
	5.1	Febetron Experiments	40
		5.1.1 Febetron Charactersitics	40
		5.1.2 Air Data	43
		5.1.3 Njtrogen Data	47
		5.1.4 Argon Data	47
	5.2	ETA Experiments	50
		5.2.1 EMP Noise and System Sensitivity	51
		5.2.2 Air Data	54
		5.2.3 Neon Data	60
6.0	REFERENCES		65
Appendices			
A	Inteferometer Signal Analysis		66
B	Phase Shift Due to Electron Density		73

LIST OF ILLUSTRATIONS

Figure		Page
1	Installation of interferometer on ETA experiment	4
2	Installation of interferometer on ATA experiment	5
3	Plan view of interferometer control room	7
4	Interferometer supports shown for ATA installation	10
5	Strongback supports shown for ETA installation	11
6	Schematic of optical strongback and vacuum vessel	12
7	High speed noise correction circuit	16
8	Schematic of control loop	19
9	Calibration signals	30
10	Detector response	38
11	View of strongback and Febetron 706 accelerator	41
12	Faraday cup signals of axial Febetron current	42
13	Line integrated electron density produced in air at 760 torr by Febetron pulse	44
14	Comparison data vs code	46
15	Line integrated electron density produced in nitrogen at 760 torr by Febetron pulse	48
16	Line integrated electron density in argon at 760 torr with 28 kV Febetron charge	49
17	Noise pickup with ETA firing	52
18	Line integrated electron density in air with 8 kA from ETA	53
19	Signals at maximum scope sensitivity with scene beam only and 8 kA from ETA	55
20	Peak line integrated electron density versus air pressure using ETA at 8 kA	57

Figure		Page
21	Beam bug signal from ETA at 8 kA with 100 torr air	58
22	Correlation between interferometer and beam bug data 50 torr air at 8 kA on ETA	59
23	Comparison of line integrated electron density on two subsequent days	61
24	Line integrated electron density in neon with 8 kA from ETA	62
25	Peak line integrated electron density versus pressure in neon with 8 kA from ETA	64

1.0 INTRODUCTION

The ATA Diagnostic Interferometer is an instrument designed to measure the electron density produced in a test gas by the intense beam of the ATA electron accelerator. It is known that the pattern of ionization produced at the head of such a beam influences the magnitude and path of return currents. Interaction of these currents with the beam has a profound effect on the stability of propagation.

Ideally, one would prefer to measure those return currents directly. In the absence of a suitable technique, measurement of the local electron density along with reasonable assumptions about the plasma resistivity and the electric field allow the return currents to be calculated.

An instrument for measuring the electron density has to meet a set of demanding requirements. It must be non-contacting because the intense, multi-pulse e-beam would vaporize a probe. It should have a subnanosecond response to resolve the fast avalanche breakdown processes occurring near the head of the beam. The sensitivity should be fine enough to detect electron-densities $< 10^{14}/cm^3$, while maintaining a dynamic range that follows the development of electron-density to $> 10^{16}/cm^3$. Finally, the instrument should be capable of operating in the hostile, high radiation, high EMP environment of the ATA experimental area.

On the basis of a previous experiment which measured similar electron-densities on a microsecond time scale, Avco Everett Research Laboratory, Inc., (AERL) proposed a visible wavelength interferometer as a viable method for fulfilling the requirements. Although visible wavelengths call for resolving on the order of 10^{-4} of a fringe, there are compensating advantages. Quiet, cw sources, and very fast detectors are readily available. Large dynamic range can be accommodated without fringe counting or other correction to the data. Finally, the advantages in aligning a visible vs infrared system are not to be discounted.

This report begins (Section 2.0) with a brief description of the interferometer and its principle of operation. A mathematical description is given in Appendix A, and the application of the principle to the measurement of electron density in particular is given in Appendix B. Sections 3.0 and 4.0 constitute an operating manual for the system. Issues of set up, alignment, calibration, sensitivity, response time, etc., are covered. Finally, Section 5.0 presents experimental data. Measurements were taken both in house at AERL using a small e-beam accelerator and at Livermore on the ETA device, which is the precursor to the ATA.

2.0 DEVICE DESCRIPTION

The instrument is separated into two major components, the control room and the optical strongback. The control room is a portable EMI shielded enclosure which is situated outside the accelerator shielding at a point over (ATA) or astride (ETA) the observation station. It contains the various elements which would be difficult to shield from radiation and EMI if placed within the tunnel. These include the laser, electro-optic, electronic, and recording components. The optical strongback is a U-shaped structure that straddles the beam line at the observation station. It is encased in a vacuum tank. On it are mounted various passive optical elements which constitute the phase sensitive "legs" of the interferometer. The phase sensing laser beam communicates between the room and the strongback.

The general layouts of these components are shown to scale in Figures 1 and 2 corresponding to the ATA and ETA configurations, respectively. Detailed descriptions of the system will follow the path of the laser beam, from control room to strongback and return to control room.

2.1 CONTROL ROOM I

2.1.1 Mechanical

The control room is a welded steel, EMI shielded module which is designed to be moved with all its contents as a single piece of equipment. To that end, provision is made for ready insertion of forklift tines under the building, and all internal components are mounted with shock isolating strapdowns. Since the module may be exposed to weather during some applications, provisions against water leakage and corrosion have been made. Ventilation is provided, but air conditioning may prove to be a necessary add on for use during the Livermore summers. The EMI shielding level with all penetrations have been specified at 100 db, and the input power is filtered to 100 db for frequencies below 10 GHz.

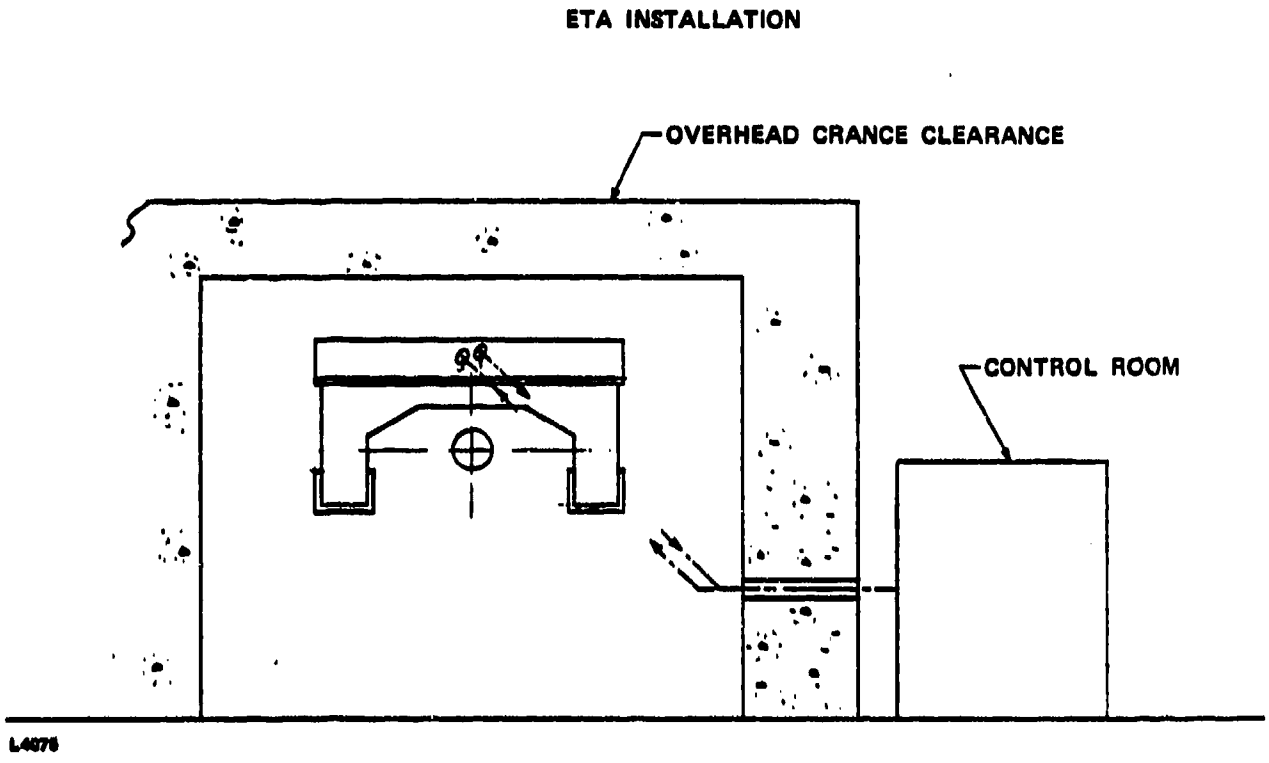

Figure 1. Installation of interferometer on ETA experiment. Interferometer is tilted to avoid overhead crane.

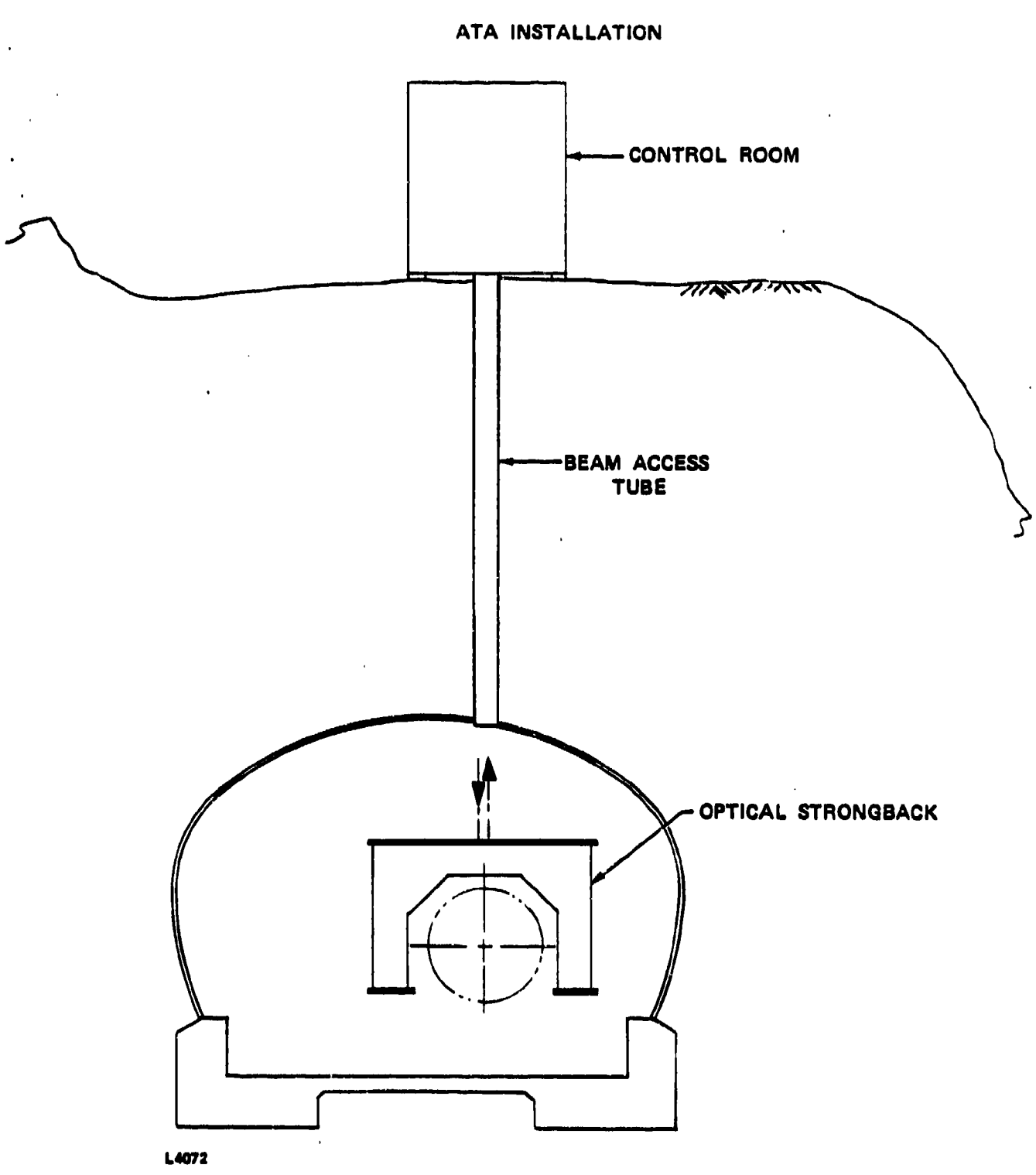

Figure 2. Installation of interferometer on ATA experiment.

The two major subassemblies within the module are the optics table and the electronics rack (see Figure 3). Space is provided within the module so that an operator may make adjustments to the optics or electronics or change film on a data recording scope mounted in the electronics rack. An operator was present continuously during ETA experiments.

The optics table is designed so as to isolate it from deflection or vibrations induced by an operator moving within the module. This is accomplished by allowing the legs to penetrate the floor of the module and so rest on their own support. These penetrations are, of course, EMI shielded. Provisions are made for retracting the table legs and locking the table and the module together for transport.

2.1.2 Laser

The laser is a Krypton ion type, Model K-3000 manufactured by Coherent Optics Corp. It is provided with an etalon for operation in a single longitudinal mode at 0.6471 micron wavelength. This provision removes amplitude noise in the 100 MHz up region which would otherwise be introduced by mode beating. The maximum output power with etalon is about 2.4 W. With clean, undarkened optics and good system alignment, only 500 mW are required. The power reserve permits the system to meet sensitivity specifications under conditions of deterioration expected for field operation.

This particular laser was chosen over similar models by other manufacturers because experiments performed at M.I.T. before purchase by Dr. Peter Pappas demonstrated the required amplitude noise level of $< 10^{-3}$ above 50 MHz.

The laser output is linearly polarized. For the purpose of understanding, the polarization may be decomposed into two mutually orthogonal polarizations of equal amplitude and, initially, equal phase. One polarization will be referred to as the scene polarization and the other as the reference polarization.

2.1.3 Electro-Optic Modulator

After leaving the laser, the beam passes through a high speed electro-optical phase modulator (Lasermetrics Model 1111). This device is used to

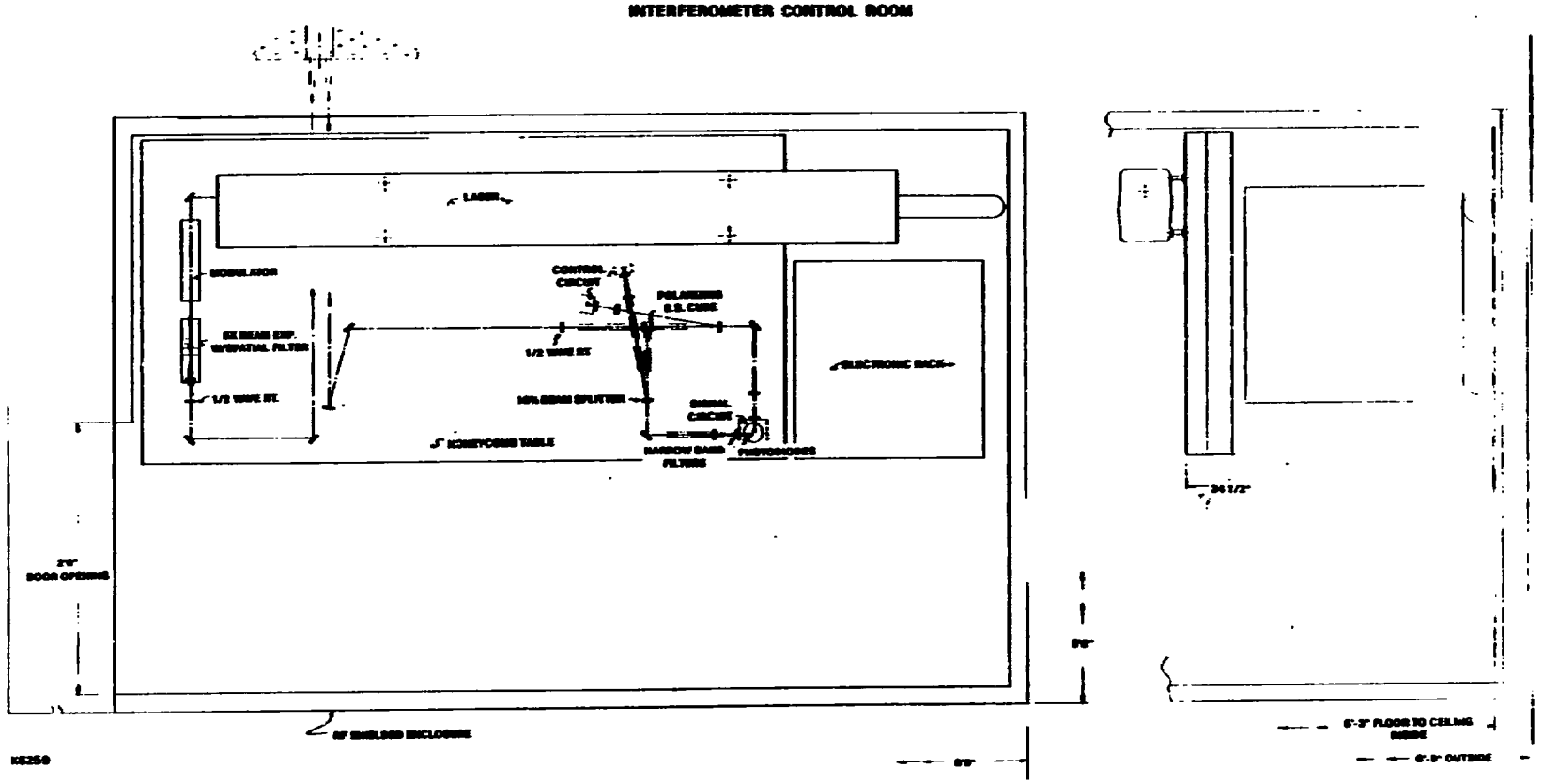

Figure 3. Plan view of interferometer control room.

impress a relative phase shift between the scene and reference polarizations. The timing of the typically 5 ns pulse is chosen such that its effect on the system output signal appears on the same oscilloscope trace as the signal due to the e-beam generated electrons. This pulse serves to provide a real time calibration of the interferometer sensitivity. The pulser employed can be triggered to 1 KHz, which will allow calibration pulses even during burst mode operation of the accelerator.

The crystal is driven by a pulser with a 1 ns rise time, which allows the system response time to be checked to 1 ns. The crystal itself is specified to have a 40 ps rise time. Hence a faster low rep rate pulser could be used to check the ultimate system speed.

After leaving the fast modulator, the beam passes through a second, low speed, electro-optical phase modulator. (Lasermetrics Model 3032) This employs several AD*P crystals arranged so as to obtain a full wave phase shift with the application of only about 200 V. The crystal C axis is so orientated that the scene and reference waves undergo maximum relative phase shift upon application of a voltage. The time dependent voltage applied to modulator is such as to maintain the interferometer continuously in balance. This action will be explained in greater detail later.

2.1.4 Beam Transport

Next a telescope is used to expand the beam by 5x to one cm (e^{-2}) diameter. At this size the beam may be transported over distances of the order of a hundred meters without further significant expansion.

Prior to exiting the room a one half wave plate is used to rotate the polarization so that, when the polarizations are separated within the optical strongback, the scene polarization and the reference polarization are properly orientated with respect to the splitting element.

The beam exits the room through a waveguide cutoff aperture in the side wall. For the ETA experiments a mirror mounted on a pedestal situated inside the concrete shielding and a second mirror mounted on top of the strongback tank directed the beam to the strongback. For the ATA experiments a mirror on a pedestal will direct the beam through a pipe extending down the diagnostic tube to the entrance aperture on the top of the strongback. The window on top of the pipe will be shielded by virtue of distance and the earth cover.

2.2 OPTICAL STRONGBACK

2.2.1 Mechanical Design

The U-shaped strongback is sized so that it will fit over the 4 ft. ATA experimental chamber. As a consequence of this size, the strongback must be mounted in tilted position so as to give clearance to the overhead crane on the ETA experiments.

Support for the strongback tank is provided by two A frames that bolt on the sides. As illustrated in Figures 4 and 5, the same frames, with the help of adapter plates, serve for both the ETA and the ATA experiments. The frame is constructed of hollow aluminum members which may be filled with sand for vibration damping. (This has not proved to be necessary.) Screw jacks are provided for leveling. These rest on vibration damping pads.

The aluminum vessel surrounding the strongback allows experiments at subatmospheric pressure without having windows directly viewing the charged particle beam. This vessel is attached to the experimental tank by means of metal bellows. Extension tubes were fashioned for mating with the smaller ETA experimental tank. Access ports are provided for adjustment of the internal components.

The optical strongback (Figure 6) is suspended within its vacuum vessel by means of a three "point" kinematic mounting system utilizing spherical bearings which are allowed to slide on rods. This system prevents stresses applied to the vessel from being communicated to the strongback.

The position of the strongback with respect to the vessel can be adjusted, by means of worm screw jacks, over a range of four inches. This allows the scene beam of the laser to be scanned across the e-beam diameter. Subsequent Abel inversion of the data will extract electron density information from the line integral. Metal bellows isolate the jacks and drives from the vacuum system.

The jacks are mated to stepping motor drives which permit remote, high resolution scanning. Experience has shown that if the stepping motors are driven at a sufficiently slow speed, complete scans can be made without disturbing system alignment. This remote capability is of particular value for ATA operations which require a substantial cooling off period before the tunnel can be entered.

ETA INSTALLATION
SIDE VIEW

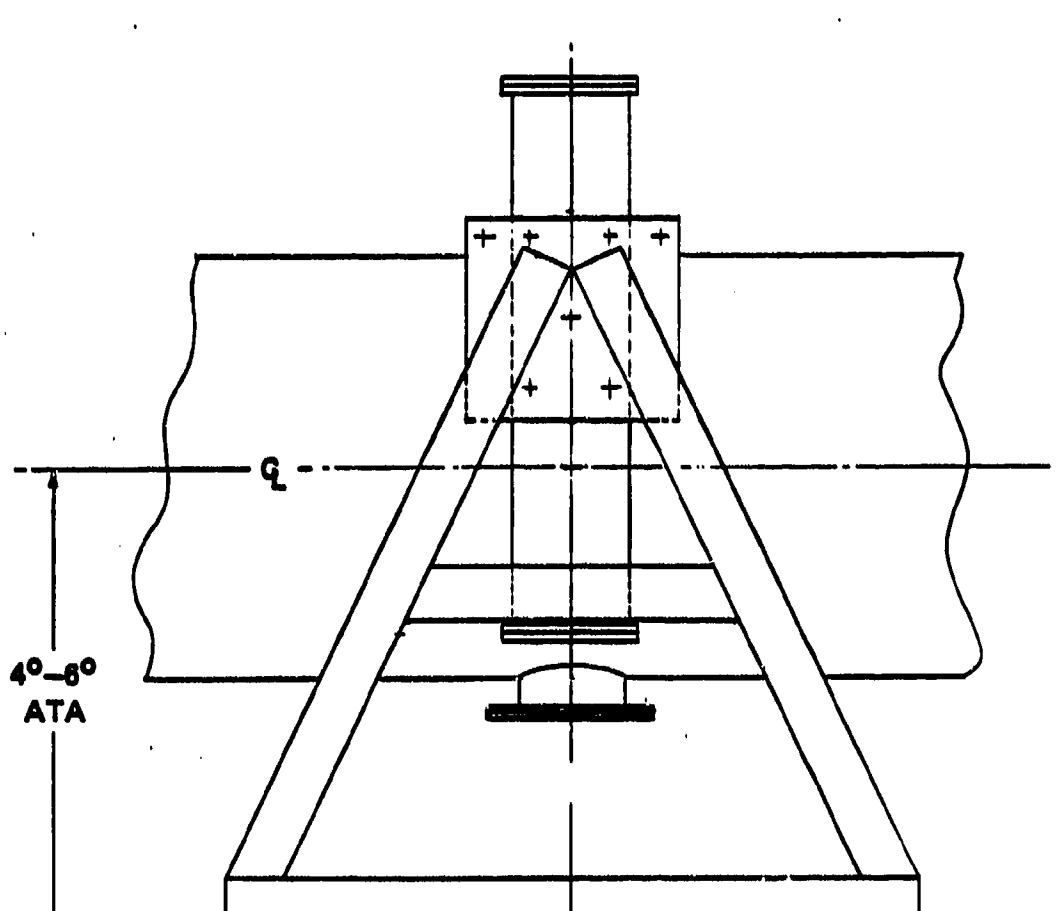

Figure 4. Strongback supports for ATA installation.

ATA INSTALLATION
SIDE VIEW

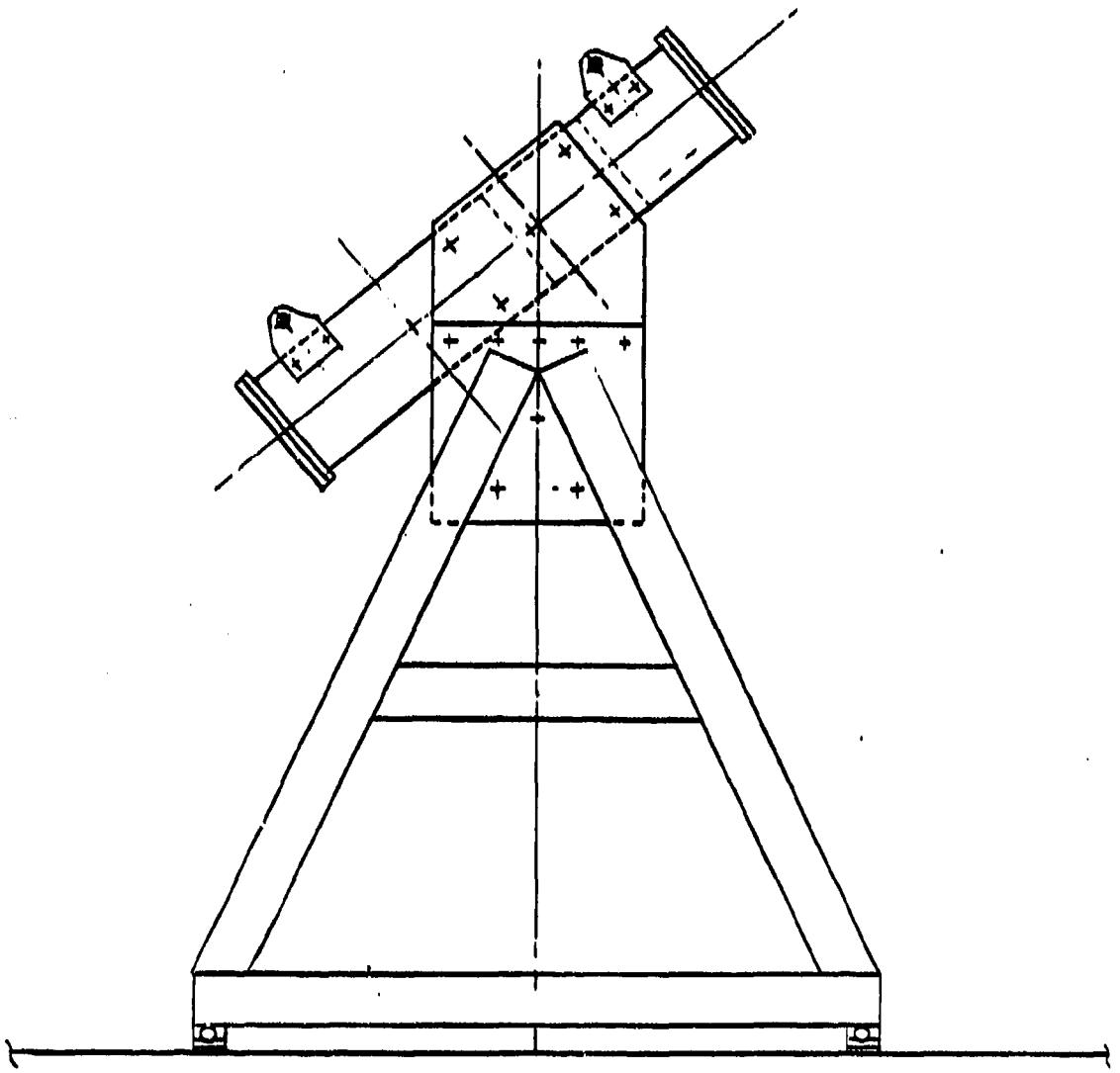

L4074

Figure 5. Strongback supports for ETA installation.

ATA INTERFEROMETER
VACUUM VESSEL & OPTICAL STRONGBACK SCHEMATIC

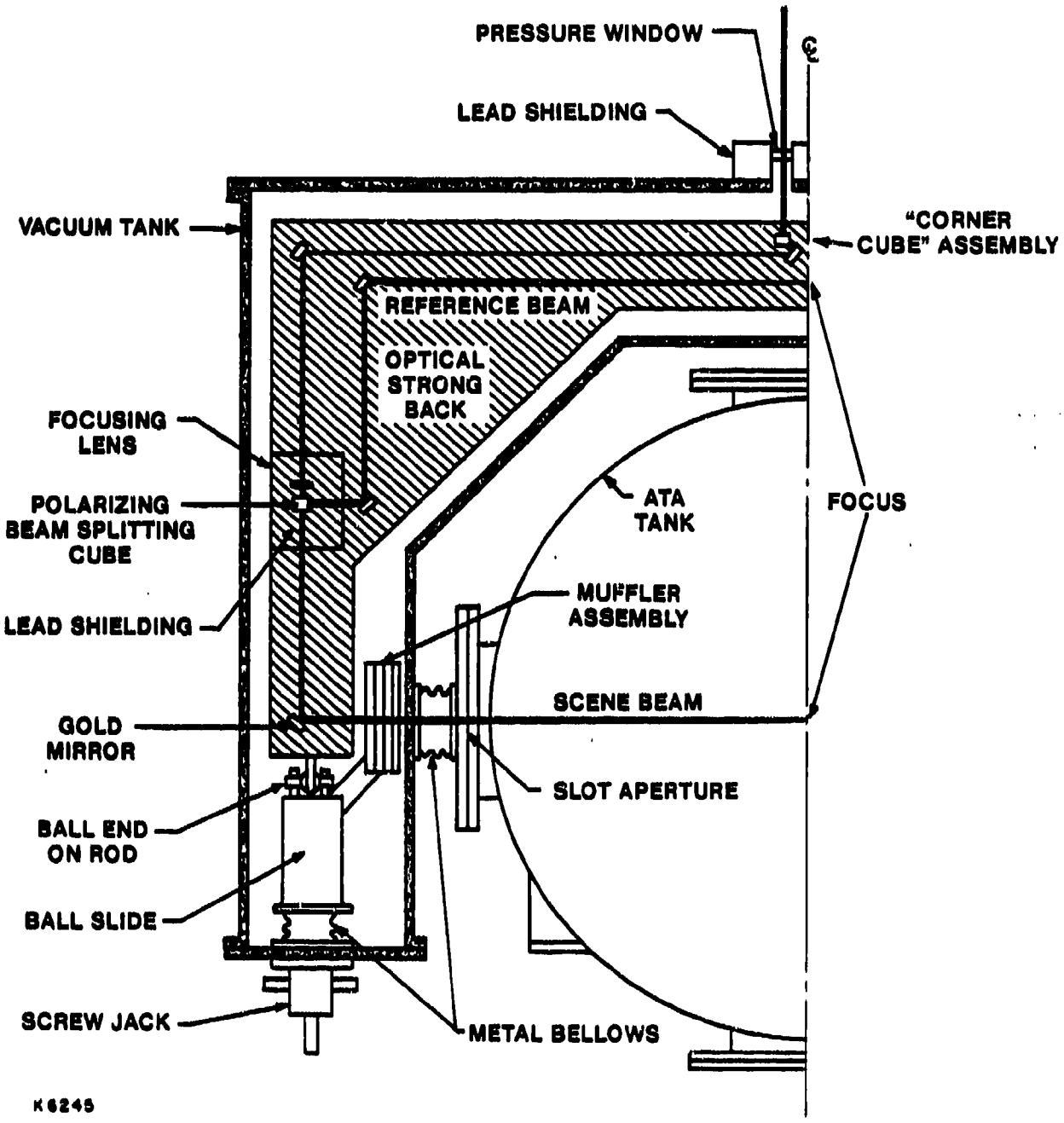

Figure 6. Schematic of optical strongback and vacuum vessel.

Calculations were made of the expected impulse and pressure on the strongback due to the cylindrical shock wave generated by the e-beam. With 1 J/cm^3 deposited by the e-beam in atmospheric pressure gas, the shock pressure at the mirror viewing the e-beam is on the order of 2×10^{-2} bar. The duration is on the order of 10^{-4} s for a net impulse on the order of one tap. Apertures mounted at the interface between the strongback tank and the experimental chamber limit the impulse area to about 1 cm^2. Taking the lower limit of 10 kg for the effective mass of an interferometer arm, an initial outward velocity of about a wavelength per second could be imparted to the arms. The electro-optic phase compensating system should easily be able to remove the effects of this motion. However, as insurance, space has been provided for installation of a muffler if further attenuation of the shock should prove necessary.

2.2.2 Optical Design

The mirrors on the strongback are configured such that the unit acts as a giant corner cube. Hence, a beam from the control room to the strongback returns to the control room parallel to the original beam. This arrangement makes the optical alignment insensitive to slight misalignments or vibrations.

Two reflections after entering the strongback assembly, the beam encounters a focusing lens which is made out of Suprasil II. The use of Suprasil II as a transmitting material is dictated by requirements for resistance to radiation damage. Immediately after the lens a polarizing beam splitting cube, which is also made of Suprasil II, is used to separate the converging beam into two polarization components. The first component has the scene beam polarization, and that component is directed across the experimental chamber such that the 0.14 mm diameter focal point occurs at the center of the test tank. The second polarization component, the reference beam, is directed through a series of mirrors over the top of the experimental chamber. On the other side of the tank, the scene beam and the reference beam are recombined into a single beam by an identical polarizing beam splitting cube. The combined beams thereafter pass through a second lens, which serves to collimate the beam again.

The focusing lens and the polarizing beam splitting cube are configured to be in close proximity to each other so that a single housing on each leg may be employed to give protection against gamma ray damage. Over three inches of lead radiation shielding is applied on all sides of these elements. The apertures which allow the laser beam to pass through these elements are orientated such that in no case do the apertures give a direct view towards the e-beam.

The issue has been brought up that the gammas produce neutrons within the lead, which could also induce damage in the optical elements. A multi-layered shielding system may be called for on ATA. Then, a neutron absorbing sandwich could be applied on the outside of the vacuum vessel.

The only optical elements that have a direct view of the e-beam interaction region are two mirrors. For two principal reasons gold has been chosen as the coating material for these mirrors. Gold should be highly resistant to any kind of radiation damage and to damage by chemical species generated by the e-beam, of which ozone is expected to be one of the most prominent. Secondly, the reflectivity of the gold is quite acceptable in the wavelength region of the laser, but it falls off rather rapidly towards the blue. This feature protects the polarizing beam splitter and the focusing lens from damage that could result from exposure to ultraviolet radiation generated by the e-beam. Gold mirrors are used in the corresponding positions of the reference beam path to maintain system balance.

2.3 CONTROL ROOM II

The laser beam returns to and reenters the control room by a path parallel to that by which it exited. The beam then passes through a second half wave retardation plate. This orients the polarization in the proper configuration for mixing the scene and the reference beams by the following polarizing beam splitter cube. A more detailed mathematical description of the mixing and detection may be found in Appendix A. What follows here is a overview.

2.3.1 Mixing

Recall that the low speed electro-optic modulator is automatically adjusted to keep the system in balance. In the absence of the high speed signal resulting from e-beam created electron density, the net retardation to the scene beam yields a circular polarization incident on the mixing cube. In effect, the phase retardation of the modulator, plus the retardation to the scene beam caused by slowly changing optical path differences between the scene and reference lens cause a net $\pi/2$ retardation. The cube splits the beam into two equal components and each of these components is made up of a superposition of light from the scene beam and from the reference beam. If a rapidly changing phase modulation small compared to $\pi/2$ is now applied by the appearance of electron density in the interaction region, then the light incident on the analyzing cube is converted from a circular polarizing configuration to a slightly elliptical configuration. (The phase correction circuit is not fast enough to respond.)

The two linearly polarized beams exiting the analyzing cube are 180° out of phase. That is, one of them will have increased in intensity while the other will have decreased by the same amount. This is dictated by conservation of energy, since the dielectric polarizing beam splitter used for mixing is essentially lossless.

2.3.2 Detection

The two beams are each brought to a focus on corresponding fast PIN photodiodes. These diodes are incorporated in a microstrip line. Electrically, the diodes are arranged in a bridge configuration (Figure 7) such that their currents subtract. As a result, an output signal is obtained that is insensitive to various perturbations such as changes in the laser amplitude, deflections of the scene beam caused by refractive index effects, or absorption of the scene beam by species created by the e-beam. Shot noise is reduced. An additional benefit is that the output signal created by the electron density induced phase change is twice as large as would be obtained if only one of the analyzed beams were utilized.

HIGH–SPEED NOISE CORRECTION

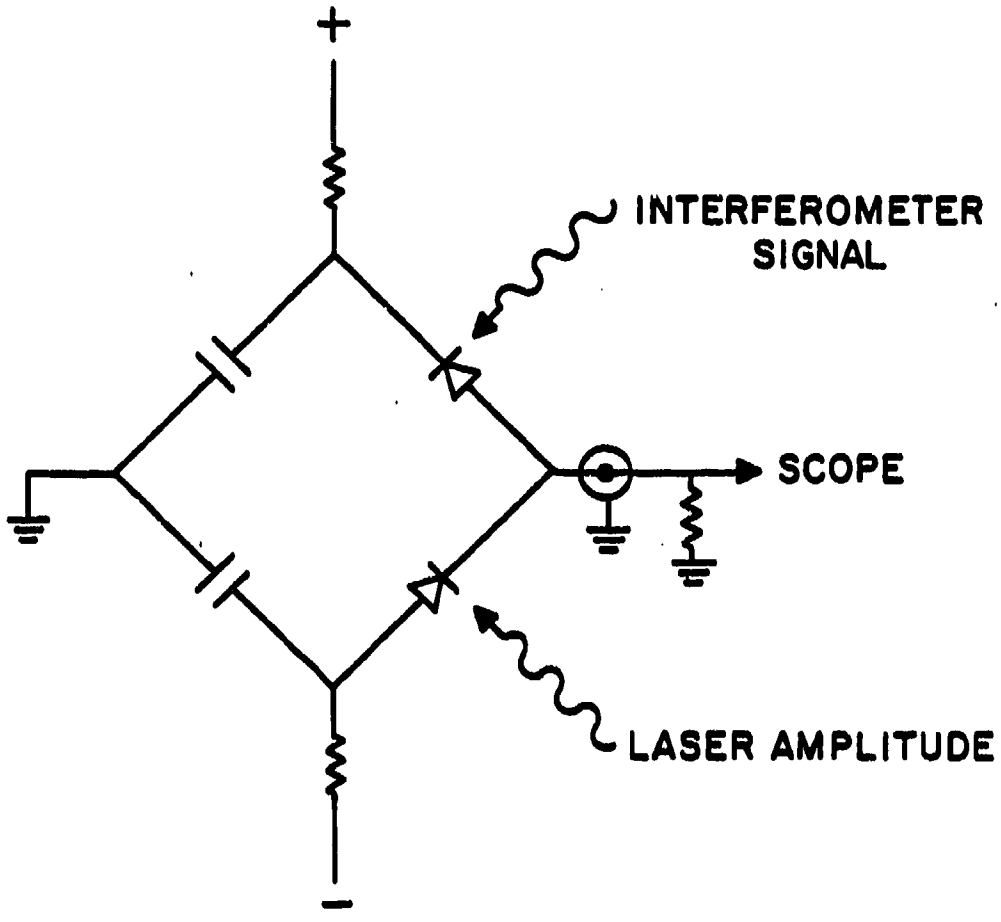

Figure 7. High speed noise correction circuit.

The power levels on the detectors was based on considerations of signal to noise and absolute signal amplitude. Photon shot noise would be the dominant factor if only one detector were used. However, with the noise cancellation of the bridge circuit, scope sensitivity determines the power. The required average power level exceeds the ratings for these diodes. To eliminate problems of diode overheating, the bias for the diodes is applied ~ 20 microseconds before the e-beam pulse and it is removed shortly after the pulse. The bias voltage is supplied by batteries within the shielded detector head. Triggering of the bias is communicated by means of an optical fiber system. These precautions are taken to eliminate any possibility of noise pickup interfering with the low levels signals.

The output from the diode bridge is passed to a Tektronix model 7104, 1 GHz oscilloscope. A coaxial line with a continuous (vs braided) outer shield from the detector head to the scope insures that any noise that exists within the screen room will not interfere with the desired signal.

Because of noise cancelling properties of the bridge, system sensitivity is limited only by the scope sensitivity. A fast, 1.2 GHz preamplifier with 7X voltage gain was added to the system to reduce this constraint, but with a $\sqrt{2}$ sacrifice in rise time. The use of battery power and careful shielding effectively eliminates EMI pickup by this component. A preamp noise level, referred to input, of 70 μV RMS is observed. Under condition of good system alignment and clean optics, this corresponds to a signal noise of ~ 1×10^{13} electrons/cm^2 RMS.

2.3.3 Control Electronics

A small fraction of each of the two analyzed beams is split off and directed towards two other photodiodes. These photodiodes, which have a relatively slow response, are used to obtain input signals to the control circuits which in turn send a signal to the modulator. Bias voltage is continually maintained on these diodes. The action of the feedback control is continuous. However, its speed is not high enough to have an effect on the nanosecond scale of the desired signal.

In its present configuration (see Figure 8 for schematic), the control circuit is able to follow disturbances as fast as one fringe/msec. This is more than sufficient to insure that the system is in balance on the first e-beam pulse.

Analysis of movies taken by N.R.L. of laser triggered channels showed that disturbances of less than 1/2 fringe within the 100 μs interframe time occurred. This puts an upper limit on the correction speed required when the interferometer is looking through channels created by a previous e-beam shot. A maximum speed of 5 fringes/msec is implied. Unfortunately the fringe rate following a single shot was not measured during the short two day data taking period available on the E.T.A. If the higher control speed proves to be necessary, a redesign of the control circuit will be necessary.

TOP LEVEL SCHEMATIC OF CONTROL LOOP

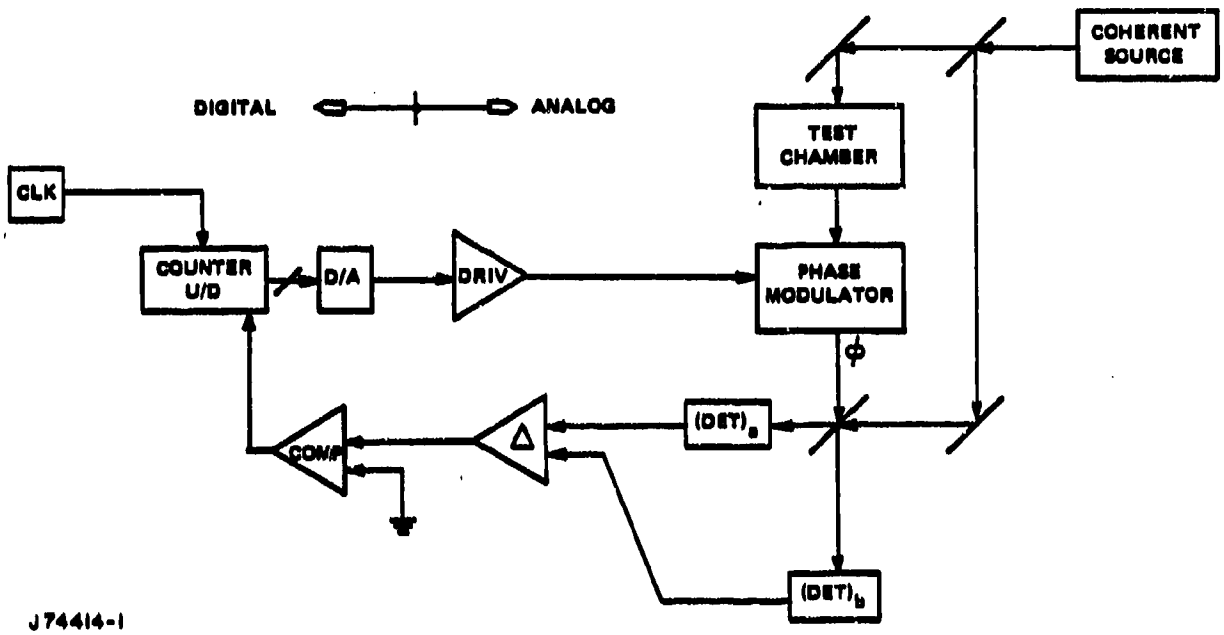

Figure 8. Schematic of control loop.

3.0 SYSTEM SETUP

Installation of the interferometer is a straightforward procedure which can be accomplished in a reasonable length of time. On the ETA tests, the total setup time amounted to six working days. This included time lost due to the necessity of recovering from shipping damage and to the fact that the ETA's test time had to be shared with FEL experiments. It is estimated that without these factors the normal setup time would be between three and four days.

3.1 ELECTRO MECHANICAL

3.1.1 Power and Water

Power and water must be hooked up to the screen room according to the specifications given in Table I. Experience at ETA indicated the wisdom of providing the water supply with a trip valve such that if the water is accidentally shut off it cannot be turned back on without a manual reset. (This avoids the possibility of laser tube damage from cold water flowing into an already hot tube). The taps on the laser power supply are then adjusted to accomodate the local voltage levels. Detailed instructions for this procedure are to be found in the Coherent laser manual.

3.1.2 Screen Room

The shock mounts, holding the optical table to the wall alongside the laser are disengaged. The cylinders projecting through the floor are turned (after loosening the lock nut) so as to lower them onto the concrete pad. The nuts on the shock mounted vertical support rods are then turned so that the table weight is transfered to the cylinders. The cylinders are adjusted so as to level the table surface at the height noted on one of the table legs. This insures that the laser beam will be at the correct height for exiting the screen room through the microwave cutoff tubes.

TABLE I SCREEN ROOM UTILITIES

Water Supply	> 8 gpm, < 40 PSI
Drain	< 10 PSI
Power	440 Vac, 80 A, 3 Phase, 60 Hz
	110 Vac, 15 A, 60 Hz
Gas	Dry Nitrogen, < 10 PSI

3.1.3 Strongback

The strongback should be positioned in the test area such that a line drawn between the center of the scene beam ports is bisected by the e-beam at the desired test point. Bellows on the pipes connecting the interferometer vacuum chamber to the test area vacuum chamber allow for misalignment on the order of up to ± 1/2 in.

Before proceeding with the optical alignment, two wooden shipping blocks must be removed from the strongback. This is accomplished by using the hand-cranks to manually raise the jacks that support the strongback within the vacuum chamber. The two jacks should be turned simultaneously to avoid tilting of the strongback which would pinch one of the blocks. The shipping blocks should be retained and repositioned under the strongback whenever the system is moved. The blocks relieve the stress on the system due to the substantial amount of lead shielding around the transmissive optical components.

The remote drive mode motors are installed on the screw jack shafts. When connecting the drive motors to the electronic drivers, care should be used that each motor goes to the driver with the corresponding serial numbers. The drivers are operated to bring the strongback into roughly mid-position in its 4 in. travel range. The limit stop lines should be installed between the strongback chamber and the drive controller to avoid the possibility of the jacks running the system beyond the mechanical range.

3.2 OPTICAL

3.2.1 Laser Turn on

Laser turn on follows the procedures given in the Coherent manual. The light power meter should be placed immediately beyond the laser output so as to prevent the beam from going through the system. No attempt to tune the mirrors of the laser to achieve output should be made for at least three quarters of an hour after turn on, since the presence of an etalon for single longitudinal mode operation leads to long thermal equlibration times. Two knobs on the equipment rack are attached to the laser feedback mirrors by means of flexible cables to allow for ease of adjustment. With some experience, the large degree of backlash can be accomodated.

Before undertaking the initial optical alignment of the system, the laser power should be reduced to less than 15 mW to avoid the possibility of damage to the KDP crystals which can result from gross misalignment. This power reduction is best achieved by misaligning the laser feedback mirror rather than by a large reduction is laser current.

3.2.2 Modulator Alignment

Angular alignment of the fast KDP crystal should be carried out first. A piece of polaroid film is orientated so as to give minimum transmission of the beam going through the fast crystal. The film is fastened over the downstream window of the fast crystal with a piece of tape. The slow KDP crystal is removed from its V block holder and a piece of white paper is taped to the input end of the 5X telescope. A mark on this paper is made at the point where the beam is transmitted through the polaroid film. Next a piece of frosted type Scotch tape is put over the entrance of the fast KDP crystal. An isogyre pattern will now be noted on the piece of white paper. The angular adjustment knobs on the fast KDP mounting are manipulated so as to center the isogyre pattern on the mark. The tape and polaroid sheet can now be removed. The power detector is placed downstream from the fast crystal and the horizontal and vertical positioning adjustments are moved so as to achieve maximum power transmission.

The slow KDP crystal is replaced in its V block mounting with the white lines at the exit aperture orientated horizontally. This should be checked with a level. The tilt and positioning controls on this mounting are then used to obtain maximum power transmission. After these adjustments the laser power can be brought up to its normal operating level, on the order of 500 MW, without fear of damage to the crystals. At this power level, fine adjustments in the vertical and horizontal direction for the fast crystal and of all the adjustments for the slow crystal can be made for maximum transmission with greater sensitivity than was done at the lower power level.

3.2.3 Optical Train

The beam exits the room through a pipe which is somewhat larger in diameter than the beam proper. The pipe can be leveled with respect to the

table surface by means of an adjustment screw on the aluminum block through which the pipe passes. If additional adjustment for alignment should prove necessary, the nut securing the pipe to the skin of the wall may be loosened, and the end moved over a small range.

A suitable set of mirrors is used to bring the beam through shielding, over obstacles, etc., so that it enters the strongback through, and roughly normal to, the window on the right (looking at the access doors) top of the chamber. No practical limitiation on the length (< 100 m) or complexity of the beam path has been identified.

The doors on the side of the vacuum chamber must be removed during the initial optical setup to allow access to the adjustments. Following the laser beam from its entrance through the window port at the top of the strongback chamber, the idea is to adjust each mirror in turn and as necessary so as to center the laser beam on the subsequent mirror. These adjustments are best carried out at first on the scene beam path with a card blocking the reference beam.

Halfway through the procedure, the scene beam may be examined after it exits the strongback chamber. The focus adjustment on the 5X telescope within the screen room is moved so as to bring the laser beam to a precise focus at the intersection with the e-beam.

Immediately before exiting the strongback, the laser beam is reflected from a one dimensional corner cube arrangement. Readjustment of this element is ordinarily not necessary. The laser beam is directed so that it re-enters the screen room centered on and parallel to the second pipe aperture. Adjustments of the optical elements within the screen room are made so as to center the beam on each following aperture through to the mixing cube.

The reference beam is then unblocked, and adjustments to the mirrors affecting its motion are made so as to superimpose this beam on the scene beam. The remotely actuated mirror in the reference beam path at the position immediately before the entrance to the beam splitting cube is then actuated from within the screen room. It will be observed that, once the scene beam and reference beam are brought to within near parallelism, interference fringes become visible. The remote adjustments are continued, finally using

the "bump" mode, so as to bring the system into a zero fringe condition. This is recognizable by increasing distance between fringes until uniform illumination is obtained.

The system is brought into course balance by adjusting the two half wave plates and monitoring light employing a power meter. The first half wave plate is rotated until an equal light power returns to the room with either the scene beam or the reference beam blocked. Balance within ± 10 percent is good enough at this stage.

Next, the second half wave plate is rotated so that, with either the scene beam or the reference beam blocked, roughly equal intensities go to the positive and negative channels after the mixing element. Once again, 10 percent accuracy is sufficient at this point.

4.0 SYSTEM OPERATION

During normal operations over an extended period, no adjustments outside of the screen room need be made. At the beginning of operations on each day the beam returning to the screen room is examined to see if the beam proper is centered with respect to the pattern of scattered light that is also transmitted through the in-pipe. If any correction proves to be necessary, it usually can be done by adjustments to the last mirror that the beam hits before exiting the room. Since the screen room and the strongback are separated from each other sometimes by large distances, and since they are set on different bases using pads which can compress at different rates, day-to-day changes in the alignment between the two components is not unexpected.

The zero fringe adjustment is remarkably stable. The system has remained in this condition for durations longer than a week without any additional adjustment. Moreover, if the remote strongback height adjustment motors are run at sufficiently slow speed the zero fringe condition will not be altered even though the strongback goes over its whole 4 in. range of travel. However, successful operation of the interferometer demands that the system be in the zero fringe condition, and this should be checked at regular intervals. Remote corrections are easily made using the motor mikes.

The remaining operations are balancing the system response and calibrating the sensitivity. These procedures are carried out at the beginning of each day.

4.1 BALANCE PROCEDURE

The positive and negative channel beams must be accurately aligned on the center of their respective high speed detectors. This is performed with the reference beam blocked so as to avoid interference effects. First the scope trace is centered with the input disconnected. The last turning mirror in the positive channel is then adjusted for highest net signal from the roughly balanced system. The fact that the system is already balanced to

within 10 percent allows high scope sensitivity to be used. The last turning mirror in the negative channel is likewise adjusted so as to give the lowest net signal.

The signal so obtained from the mirror adjustment with scene beam only is recorded as (arbitrary units - volts or current) ΔI_S, which may be either positive or negative. The scene beam is then blocked and the corresponding signal, ΔI_R, with the reference beam only is noted. The second half wave plate is then adjusted to bring the difference signal to the level $(\Delta I_S + \Delta I_R)/2$.

Next, the variable attenuator on the negative channel is adjusted to bring the difference signal to zero. This is accomplished by rotating the third half wave plate. A small fixed attenuation may be necessary in the positive channel to bring the system within range of the variable adjustment. (This is readily accomplished with glass slides taped over the entrance hole leading to the positive detector.)

Upon switching back to the scene beam only, the difference signal should remain zero. If it is not, an iteration of the process of adjusting the second half wave plate followed by an adjustment of the variable attenuator is called for.

The rationale for the above procedure is apparent from inspection of Eq. (A-13). With the respective beams blocked, the difference signals are:

$$\Delta I_S = \frac{A_S^2}{4} [\delta Q + 2Q \sin 2\Delta]$$

$$\Delta I_R = \frac{A_R^2}{4} [\delta Q - 2Q \sin 2\Delta]$$

The average of these signals

$$\frac{\Delta I_S + \Delta I_R}{2} = \frac{(A_S^2 + A_R^2)}{8} \delta Q + \frac{A_S^2 - A_R^2}{4} Q \sin 2\Delta$$

is generally dominated by the error in sensitivities ($\delta Q \neq 0$); that is, the first term dominates when the system is in rough balance with $A_s \sim A_r$ and $\Delta \sim 0$.

Hence, if the angle Δ is adjusted to bring either ΔI_S or ΔI_R to this average value, then to first order they both must approach this average value. A subsequent sensitivity balance adjustment ($\delta Q \rightarrow 0$) will bring them both to near zero.

For the final step in the balance procedure the values of the scene beam only and reference beam only signals are noted with the negative channel blocked. If they are not equal, they are adjusted by means of the first half wave plate until they are so. Accuracy of a few percent is sufficient. Inspection of Eq. (A-13) shows that this adjustment only affects the third term since the first two are zeroed in the balance procedure. The product $A_S A_R$ is thereby maximized, giving maximum sensitivity.

In typical practice, signal levels from either the scene or the reference beams into a single channel are on the order of a couple of hundred mV. The balance procedure is readily carried out to a few mV. After a day's operation with no further adjustments, the balance is usually still within ± 10 mV. (It is expected that drift is due to displacement of the beams on the fast detectors, which introduces a δQ. This has not been systematically investigated.) Hence, the assumed value of $\delta Q/Q < .1$ of Eq.(A-19) is experimentally justified.

4.2 CALIBRATION

The sensitivity of the system is known if we can determine the parameter V_p, the maximum output voltage of the system when it is forced through a phase shift of $> \pi$ rad (see Appendix B, Eq. (B-6)). There are several ways of forcing the system through the required phase shift. With both methods the automatic phase compensation must be turned off.

In the first technique, hot air from a heat gun is blown across the scene beam. The detector bias and the scope trigger are driven at 10 Hz repetition rate using a pulse generator. The scope camera shutter is allowed to remain open long enough to record a number of traces. This is illustrated in

Figure 9a. The parameter V_p is simply 1/2 the difference between the highest and the lowest voltage level recorded.

Figure 9a shows steps in the traces which are due to pulsing of the fast modulator with a fixed voltage signal. Note that the amplitude of these steps goes to zero as the traces approach their maximum or minimum values, as expected. Note also that both positive and negative excursions are observed. This is a consequence of the fact (see Eq. (A-15)) that for any given phase shift ϕ, a phase shift of $\phi + \pi$ will give the same output; however, the derivative of the output voltage with respect to small changes in ϕ will be opposite in the two cases. Of course, when the feedback controller is on the system is locked at a single phase point, roughly $\phi = 0$, and the sign of the response always remains the same. The controller is set up so that electrons will always give a negative signal.

When the interferometer is hooked up to the ATA test tank, the scene beam will not be readily accessible. Moreover, because of radiation levels within the tunnel, it will be desirable to do the calibration entirely by remote means. To this end the slow modulator, which is ordinarily used for feedback control, can be driven so as to impress a greater than 2π phase shift on the system. Figure 9b shows the result of driving the modulator with a sawtooth voltage. The details of the complex wave form are unimportant. As before, V_p is obtained from 1/2 the peak to peak signal observed (the decay of peak to peak amplitude beginning at roughly 40 μsec is due to removal of the bias voltage to the detectors).

We have already mentioned how the fast phase modulator is used to insure that the calibration is known through the course of an experiment. Any change in the amplitude of the calibration pulse, which is superimposed on a data pulse trace, is used to modify proportionately the assumed value of V_p which is employed for calculating the electron density.

Given the manufacturer's specified half-wave voltage for the modulator along with the applied voltage pulse and the response of the system to that pulse, one should be able to calculate the system sensitivity factor V_p. The parameter V_p is given by

CALIBRATION SIGNALS

A)

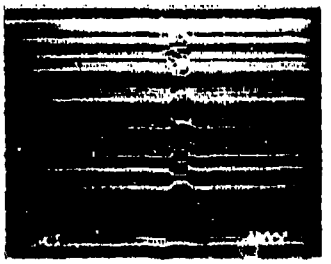

SCENE BEAM
PHASE DISTURBED
BY HOT AIR GUN

10 ns/div

B)

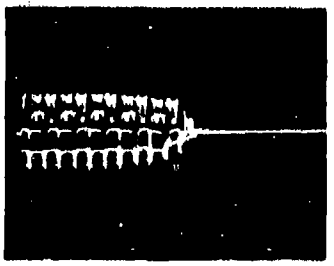

MODULATOR DRIVEN
WITH SAWTOOTH
VOLTAGE

10μ s/div

L4087

Figure 9. Calibration signals. (a) scene beam phase disturbed with hot air gun with superimposed modulator pulse. (b) Modulator driven with saw tooth voltage.

$$V_p = \frac{V_{1/2}}{V_M} \frac{V}{\pi}$$

When this is done, a value of V_p is obtained which is roughly 1/2 of the value that is directly measured. Possible explanations for this result are misalignment of the fast modulator crystal, or a half-wave voltage that is roughly twice the quoted value.

No fault could be found with the alignment of the crystal. The crystal has been returned to the manufacturer for a check on the half-wave voltage (and also on a transmission which is considerably below specification). With a dc applied voltage the manufacturer claimed that the device is within specifications. They claim a ~ 10 percent increase of $V_{1/2}$ is expected for short pulses. Other experience (private communications from expert at U of Rochester) has given a 40 percent increase in $V_{1/2}$ for nanosecond pulses. These figures are still below our observations of a 100 percent increase. Hence, for the moment, the cause of this discrepancy remains a mystery.

One other explanation for the above behavior would be that one of the two detectors became damaged in a way such that it ceased to have a high speed response while its low speed response remain unchanged. Using the value of V_p inferred from the slow speed calibration test one would then infer a value for the half-wave voltage that was a factor of two too high. In fact, the true problem would be that the value of V_p appropriate to fast signals was a factor of two too large. If this is indeed the case, then all values of line integrated electron density which are to be quoted should be multiplied by a factor of two. The quoted RMS noise in line integrated electron density would be unchanged since this factor appears to be dominated by preamplifier noise.

At the time of this writing the apparatus is at Livermore and is unavailable to the author. When preparations are made for the ATA test, the detectors will be checked to see if either had lost their high speed response.

4.3 POWER LEVELS AND SENSITIVITY

In this section we discuss the typical operating parameters encountered both at Avco Everett Research laboratory and after shipment to Lawrence Livermore Laboratory. The four principle factors affecting system sensitivity are: 1) laser power, P, 2) system transmission, T, 3) detector response, Q, and 4) fringe contrast, C. The peak output voltage, V_p, obtained in the calibration procedure of Section 4.2 is related to these factors by:

$$V_p = P\ T\ Q\ C\ 50\ \Omega$$

Each of these factors will be treated in turn.

4.3.1 Laser Power

The laser normally is capable of 2.4 W out in a single longitudinal mode. During operation at AERL an output of 0.5 W was sufficient to give the desired system sensitivity. The laser was normally operated in the "light control mode" which maintains this power level despite drifts in internal laser alignment.

(After roughly six hours operation the drift becomes too large for the automatic control, and the laser current pegs at maximum. Manual adjustment of the rear mirror using the flexible cable control is then carried out so as to bring the current to a minimum. This is done with the system still under light control.)

During shipment to Livermore, a mote within the laser discharge tube broke loose and lodged in the center of a Brewster window. This caused the maximum output power to be reduced to about 0.5 W. Since there was no longer any power reserve, the light control mode would not function near that level. The experiments were conducted between 0.38 and 0.48 W.

4.3.2 Transmission Factors

After leaving the laser, the beam passes through or reflects from some 55 uncontacted surfaces. Table II details the optical train of a ray that passes through the reference leg of the strongback and the positive leg of the

TABLE II - OPTICAL TRAIN

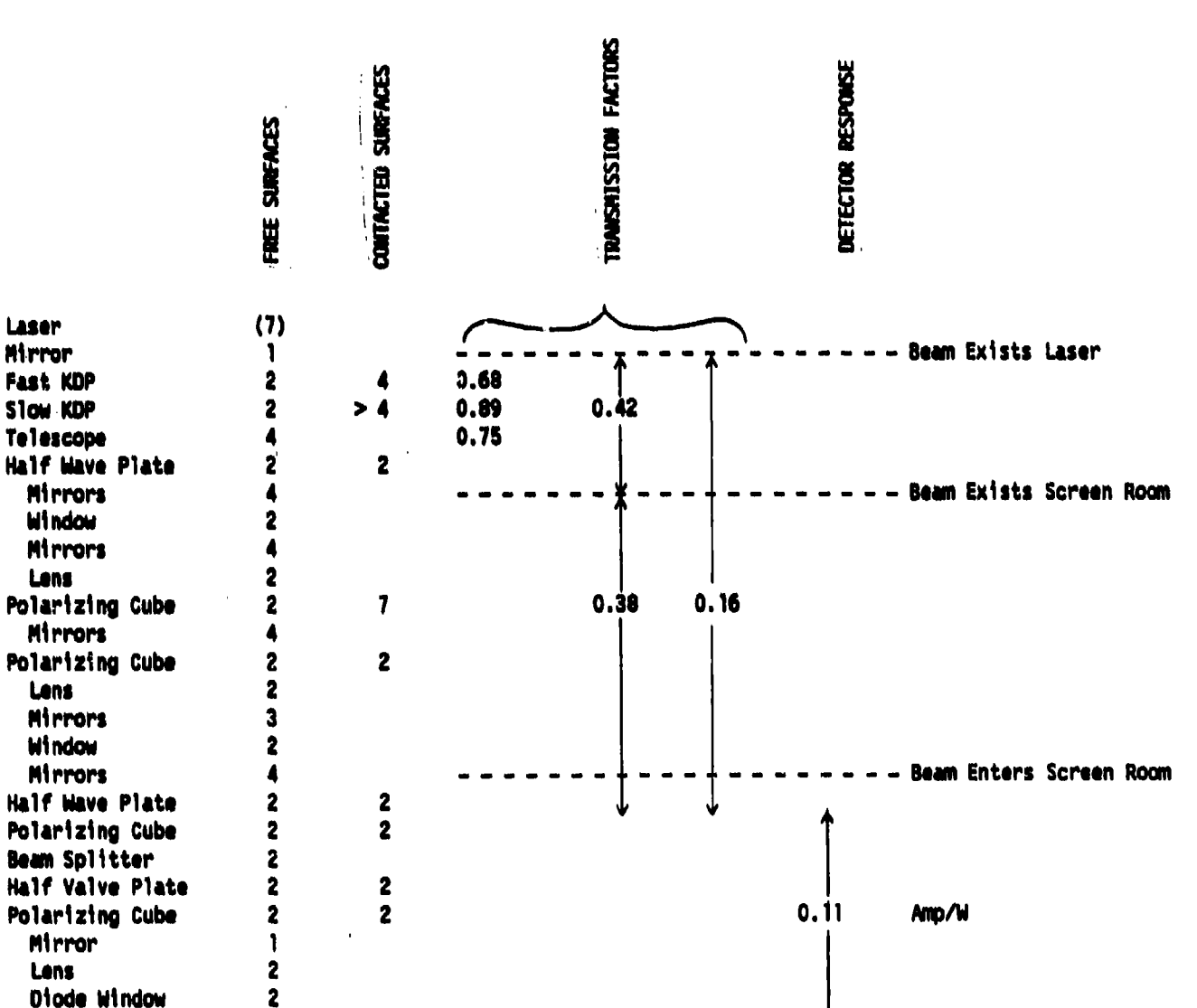

detector. Of these surfaces, all but four are exposed to accumulation of dust and polluting films. Nonetheless, the transmission did not change substantially during experimentation at AERL or after shipment to Livermore.

The first major loss is through the fast KDP modulator. Roughly 10 percent is due to aperture scraping. Taking into account that factor, the crystal transmits ~ 78 percent while it should be transmitting ~ 90 percent. It has been returned to the manufacturer to correct the problem.

The slow KDP modulator transmits roughly as expected or 84 percent. The transmission of the expanding telescope is a poor 75 percent. Improvements in this factor should be possible through better coatings.

The beam leaving the room had, at AERL, typically 42 percent of the laser power. This will be referred to as the "exit transmission". At Livermore, the average figure was a point or two lower indicating minimal degradation in transit.

At AERL, about 38 percent of the beam leaving the room managed to pass through the various optical elements and return to the room to the standard measurement station immediately after the second half wave plate. This will be referred to as the "external transmission." The single biggest loss, ~ 5 percent, occurs on one of the windows to the strongback, which has a defective coating.

For the Livermore experiments on the E.T.A. it was decided to use windows on the test chamber rather than connect the strongback chamber through extension pipes to the test chamber. This was done to save time. The test chamber pump down circuit was not fitted with a cold trap. Cold trapping provisions would have had to be made in order to avoid contamination of the optics internal to the strongback chamber.

Since these windows did not have an anti-reflection coating, an additional 20 percent loss could be expected. In fact, an external transmission of 31 percent was measured, which is of the right order. (No extensive cleaning of optics after shipment to Livermore proved necessary.)

At the end of the first day's operation on E.T.A. the external transmission was measured at 25 percent, and an unbalance between scene beam and reference beam power noted. The next morning a figure of 19 percent was obtained. The windows were visibly darkened by the radiation.

Substitution of fused silica windows (Corning 7940), which are radiation resistant, brought the external transmission up to 27 percent. Towards the end of the second (and last) day of the Livermore measurements, the overall transmission declined such that the external transmission would be 21 percent if other factors, (not checked) had remained constant. Variations of laser output during these measurements introduces some uncertainty as to whether the silica window had darkened.

The "overall transmission" is the product of the "exit transmission" times the "external transmission." At AERL it had a value of ~ 16 percent and declined to a low of ~ 10 percent at the beginning of the second day of Livermore experiments.

4.3.3 Detector Response

The laser powers are too low for accurate measurement with the Coherent power meter beyond the point where the scene and reference polarization are mixed. A measure of performance is obtained by dividing the power beyond the second half wave plate into the sum of the absolute values of the currents from the positive and negative detector channels. This gives an effective response in amps/W. This figure, of course, includes not only the inherent detector response (0.24 A/W, typical spec) but also factors in attenuation of remaining optical elements, focussing, and alignment. Effective response figures of 0.11 A/W were observed both at AERL and Livermore. Based on the specifications, a 46 percent, "final transmission" factor is operative. The specific contributors to this factor were not analyzed.

4.3.4 Fringe Contrast

It is interesting to obtain a measure of what fraction of the photocurrent is actually contributing to the useful signal. Denote by V_R the signal obtained with the reference beam, (scene beam blocked), going into only one channel. Likewise, let V_S be the signal obtained with the scene beam only, once again going into only one channel. Of course, if the system is balanced, V_R and V_S will be equal. Consider now the case where both the scene and reference beams are unblocked and the phase is adjusted so that signal V_p is observed. Then the interference between the scene and reference beams are

such that all the light should be going into the positive channel. The voltage, V_p, should then ideally be equal to twice the sum, $V_R + V_S$. There are factors which could cause the result to deviate from this ideal situation. For instance, the wavefront of the scene beam could be curved with respect to that of the reference beam so that perfect interference across the wave front is not obtained. A measure of the quality of interference between the two beams can be expressed as

$$C = \frac{V_p}{2\,(V_R + V_S)}$$

The results of putting values measured at AERL into this expression gives a value of C = 0.92. That is, the obtained fringe contrast deviates from the ideal value of 1 by a factor of about 8 percent. This performance is judged to be quite good.

As has been mentioned, windows were used in the scene beam path during the ETA experiments at Livermore. The thickness of the window was such as to introduce an estimated half wave curvature across the scene beam profile. This curvature results from the increase of optical path length between the two lenses on the strongback which are separated by a confocal distance.

Since the reference beam does not undergo a compensating distortion, the interference between the two beams can be expected to be reduced. The measured value of the contrast ratio was 0.73. Hence, this portion of the degradation introduced by the window is quite tolerable. For applications in which windows are normally desired, the degradation of contrast ratio could easily be avoided by introducing compensating windows in the reference leg.

4.3.5 Detector Response Time

The detector package was designed to make use of high speed PIN photodiodes manufactured by Hewlett Packard. The specific model number is HP5082-4205. The devices are mounted in a small, 1.5 mm, leadless package which allows them to be incorporated in a microstrip line circuit for high speed response. With a 20 V back bias, these devices should have a response time better than 1 ns.

Early on in the program this response time was checked with the diodes mounted in their final circuit configuration by illuminating them with the output from a pulsed laser diode. The results of this test are shown in Figure 10a. On this trace, the 10 to 90 percent rise time is on the order of 600 picoseconds.

Initial experiments performed using the Febetron as an electron density source showed extremely small signal return and a very slow signal rise time. A loss of detector response time was on the list of possible explanations. The tests were repeated using the pulsed laser diode, and the results obtained in the last figure were again obtained. To resolve the problem, a fast modulator was purchased since this would allow an independent check of the detector system response using the system's laser for illumination. In trace (b) we show the voltage applied to the fast modulator. The corresponding detector signal had a rise time on the order of 50 ns.

After a number of tests, it was discovered that the detector response time depended on how the detector was illuminated. If the detector was removed from its housing so that the laser diode could illuminate it from an angle, it was found that the slow response time could also be achieved with laser diode illumination.

The detector packages are fabricated with an integral glass lens. Inside the package there resides a square silicon chip. The whole surface of this square is photoactive on a dc basis; however, it turns out that only a central circular area has the desired high speed response. This central circle occupies roughly 10 percent of the chip area. The integral lens acted so as to focus the light from the diverging laser diode, placing it quite precisely on to this high speed area.

Unfortunately, similar results could not be obtained with the converging beam used with the interferometer. However, improvements from our initial results were achieved by carefully moving the focal point of our converging lenses and varying the position of the focal spot on the detector. The best results obtainable using these techniques are shown in Figure 10c. The rise time is on the order of 10 ns using both detectors in the differential mode. It was likely that this poor performance was due to the presence of the integral lens which either scattered or refracted some of the beam onto the slow response area. Attempts were made to remove the lenses from the diodes, but this was not achieved without fatal damage to the devices.

DETECTOR RESPONSE

A)

HP5082–4205 RESPONSE TO LASER DIODE ILLUMINATION

B)

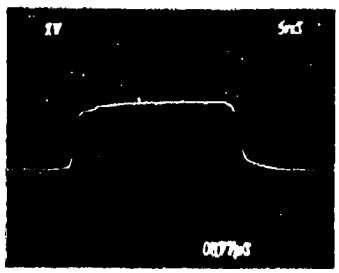

VOLTAGE TO FAST MODULATOR

C)

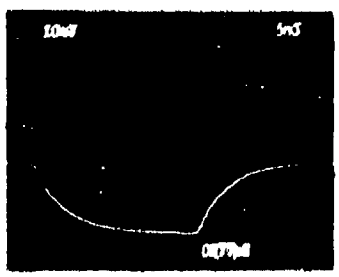

HP5082–4205 RESPONSE TO PHASE MODULATION

D)

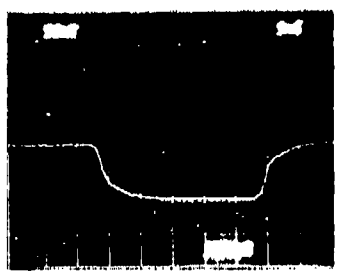

MOTOROLA MRD510 RESPONSE TO PHASE MODULATION

L4091

Figure 10. Detector response. (a) response of HP 5082-4205 detector to laser diode illumination. (b) voltage to fast modulator. (c) response of HP 5082-4205 detectors to phase modulation. (d) response of Motorola MRD 510 detectors to phase modulation.

The rise time obtained with the Hewlett Packard diode was judged to be insufficient for the rapidly approaching ETA experiments. As a stop gap measure, we fabricated a new detector bridge board with diodes manufactured by Motorola, MRD510. These detectors have leads, and hence could not be incorporated in the stripline as were the Hewlett Packard diode. Once again employing 20 V back bias, the response time was tested using the modulator. The results are shown in Figure 10d. There appears to be two components to the rise time. A fast component occupying roughly 2/3 of the amplitude occurs on a scale of somewhat less than 2 ns. Subsidiary slow rise on the order of 5 ns is noted for the final third. Although this response is considerably slower than the original program objective of 1/3 ns, as the subsequent data taken with the Febetron 706 and on ETA will illustrate, it was adequate for the initial experiments.

We believe that it will be straightforward to achieve our initial goal of 1/3 ns response time. To this end, we have placed a special order to Hewlett Packard for detectors without the integral lenses. Some will be bare and some will have a plain window.

To achieve 1/3 ns, bias voltage will have to be increased. Hewlett Packard has informed us that the rise time should scale as one over the bias voltage to the 0.76 power and that reverse biases as high as 200 V can be tolerated. A reverse bias of 100 V should be sufficient to obtain the desired rise time. Modification of the pulsed biased circuit to achieve this will be necessary.

5.0 EXPERIMENTAL RESULTS

5.1 FEBETRON EXPERIMENTS

Initial checkout experiments on the interferometer were carried out at Avco Everett Research Laboratory using a Febetron 706 accelerator as an e-beam source. The accelerator was positioned to fire across the scene beam. Figure 11 is a photograph of the setup. The Febetron was mounted on tracks so that the distance between the output foil and the scene beam could be readily varied.

A lead housing was placed over the output end of the Febetron so that experiments could be carried out in different gases. Slots in the side of the housing allowed the scene beam to pass through. Test gases were introduced at atmospheric pressure through a hole and allowed to flow out the slots. Before conducting an experiment the test gases were allowed to flow for a sufficiently long time to assure good purging of the housing. Experiments were conducted using air, nitrogen, and argon, all at atmospheric pressure.

5.1.1 Febetron Characteristics

The Febetrons 706 accelerator is rated to put out a maximum of 10,000 Amp at 600 keV energy. The nominal pulse time is 3 ns. Unfortunately, not all of these characteristics were amenible to direct measurement. Moreover, no calibration curves were provided for the output voltage. Since the device is based on a Marx bank, a first order assumption is that the output voltage will be proportional to the charging voltage divided by the maximum allowable charging voltage (30 kV) times the 600 kV figure.

Measurements of the on axis current density were carried out using a Faraday cup in front of the output foil. The Faraday cup had a 2.54×10^{-3} cm^2 hole. Figure 12 shows the recorded signal under two conditions of charging voltage through the Marx bank. At 25 kV charge, double pulse behavior was observed with slightly over 30 ns between the first pulse and the smaller second pulse. This double pulse behavior could be of interest

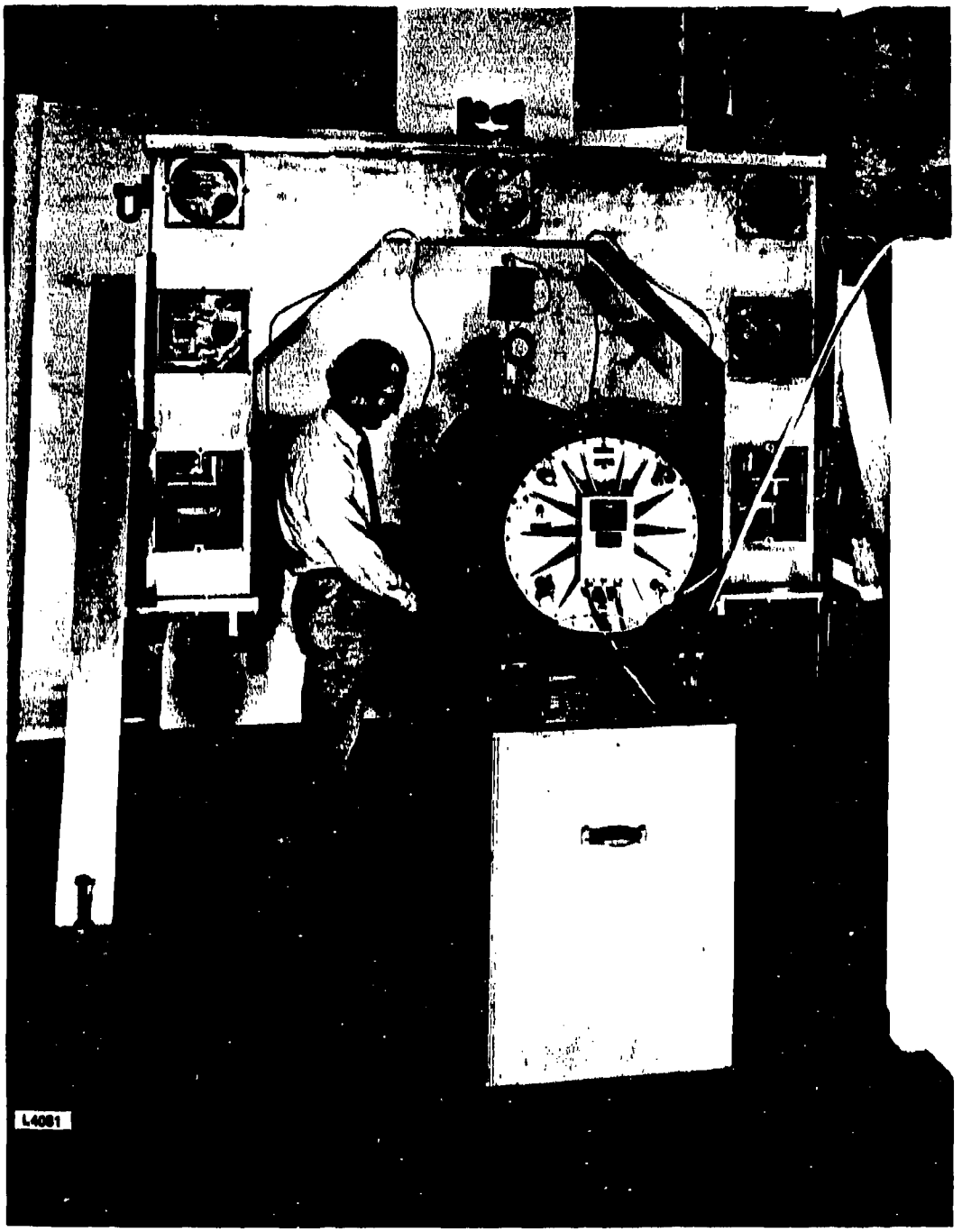

Figure 11. View of strongback and Febetron 706 accelerator in place for electron density experiments.

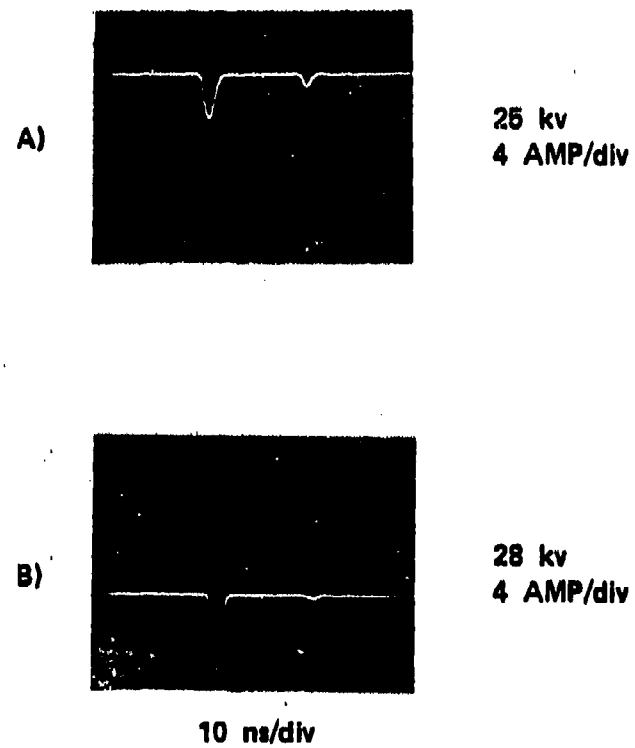

Figure 12. Faraday cup signals of axial Febetron current transmitted through $2.54 \times 10^{-3} cm^2$ hole for two Marx bank charging voltages.

for CPT studies. With a slight increase of voltage to 28 kV the second pulse almost disappears and a substantial increase in the first pulse occurs. It will also be noted from the figure that the pulse width of the first pulse decreases somewhat, yielding a full width at half maximum on the order of the 3 ns claimed for the system. The axial current density for the shot shown is about 4 kA/cm^2.

A rough check on the beam diameter was obtained by taking a 10 shot overlay using blue cellophane taped to the output foil. A beam diameter on the order of 1.5 cm to 2.0 cm is obtained. If the current density were roughly uniform over the 1.5 cm diameter, then the 28 kV shot would correspond to a total current of on the order of 7 kA.

5.1.2 Air Data

The first set of experiments were carried out using laboratory air. Relative humidity measurements were not made at the time. However, a value of 20 percent was typical for the lab. The Febetron was positioned so that the scene beam crossed the e-beam at a distance of 2 cm from the foil. This was done to allow the e-beam, which originates from staple like protrusions in the diode, to be scattered by the foil. The scene beam was centered on the e-beam.

Figure 13a records the phase shift occurring with a 28 kV charge to the Marx bank. The scale is such that one full division corresponds to 1.05×10^{15} (electrons/cm^2)/division. The first pulse seen on the figure is due to the main e-beam pulse. This is followed ~ 30 ns later by a small additional signal caused by the second e-beam pulse. The large third pulse occurring in the figure is due to a calibration signal applied to the fast electro-optic modulator.

The fast rise time of the first pulse apparent in trace (a) is resolved in trace (b) which was taken on a subsequent shot at a faster 5 ns sweep speed. The rise time of the electron density is on the order of the e-beam full width at half max, or 3 ns.

The last trace in the Figure 13c, shows the signal obtained with the reference beam blocked. Note that the scene beam is still crossing the e-beam. From the trace it is impossible to tell when the e-beam was fired. This demonstrates that all the signal shown in Figure 13a is due entirely to phase shift effects, as opposed to absorption or beam steering.

AIR 760 TORR

$n\ell$ = 1.05 x 10^{15} (ELECTRONS/cm^2) /div

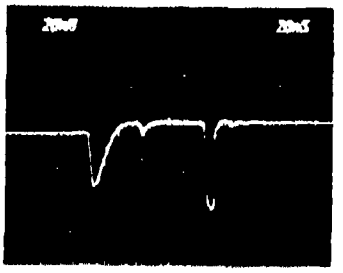

A) 28 kV

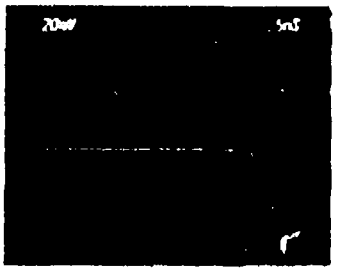

B) 28 kV

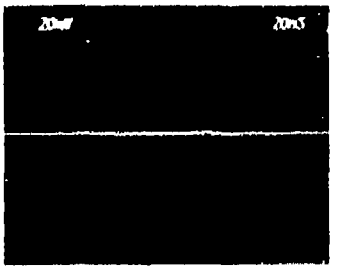

C) REFERENCE BEAM BLOCKED

L4089

Figure 13. Line integrated electron density produced in air at 760 torr by Febetron pulse. (a) Febetron charged to 28 kV. (b) Same conditions as (a) but high sweep speed. (c) Same conditions as (a) but reference beam blocked.

Returning to the top trace (a) in Figure 13, it will be noted that the baseline does not return to zero after decay of the electron density. Rather a phase shift corresponding to ~ 30 percent of that produced by the peak electron density, but of opposite sign, is observed. It is believed that this effect is due to the presence of metastable excited states.

The presence of these excited states was anticipated as a factor which would cloud the interpretation of late time phase shifts using visible wavelength interferometry at one color only. We have made crude arguments that at early times, when the e-beam is on, the rate of promotion of electrons to the continuum is considerably greater than that to any particular excited state. Hence, the phase shifts during these early times should be dominated by the free electron density, except in pathological cases where an excited state transition was very close to the probing laser frequency. It is, of course, the resolution of the early time electron density which has motivated the technical approach we have followed.

This data may be compared with theoretical predictions. A.W. Ali of the Naval Research Laboratory was kind enough to do a computer run on the electron density expected from a 6 kA beam of 600 kV with a uniform 2 cm diameter and a triangular pulse profile of 2.5 ns up and 2.5 ns down. These figures correspond roughly with the expected Febetron 706 output. The data of Figure 13b is presented in blown up form in Figure 14. Overlaying that data, we present the results of these calculations scaled so that the peak of the data and the calculations match. This scaling correspond to taking the current density, 1.9 kA/cm^2, of Ali's calculation to be uniform over a 1.36 cm diameter. As measured by the Faraday cup, the peak Febetron current density was of 4.3 kA/cm^2, and it extended over roughly 1.7 cm diameter with a distribution that was not known. If the distribution were uniform, then the measured density would be a factor of 2.8 less than the expected density.

Of particular interest is the close agreement in the profiles of theory and experiment during the rise of electron density. A line integrated electron density of $10^{14}/cm^2$ is readily resolved. At the peak of the distribution the data shows a glitch. Similar glitches were seen in some of the Faraday cup data.

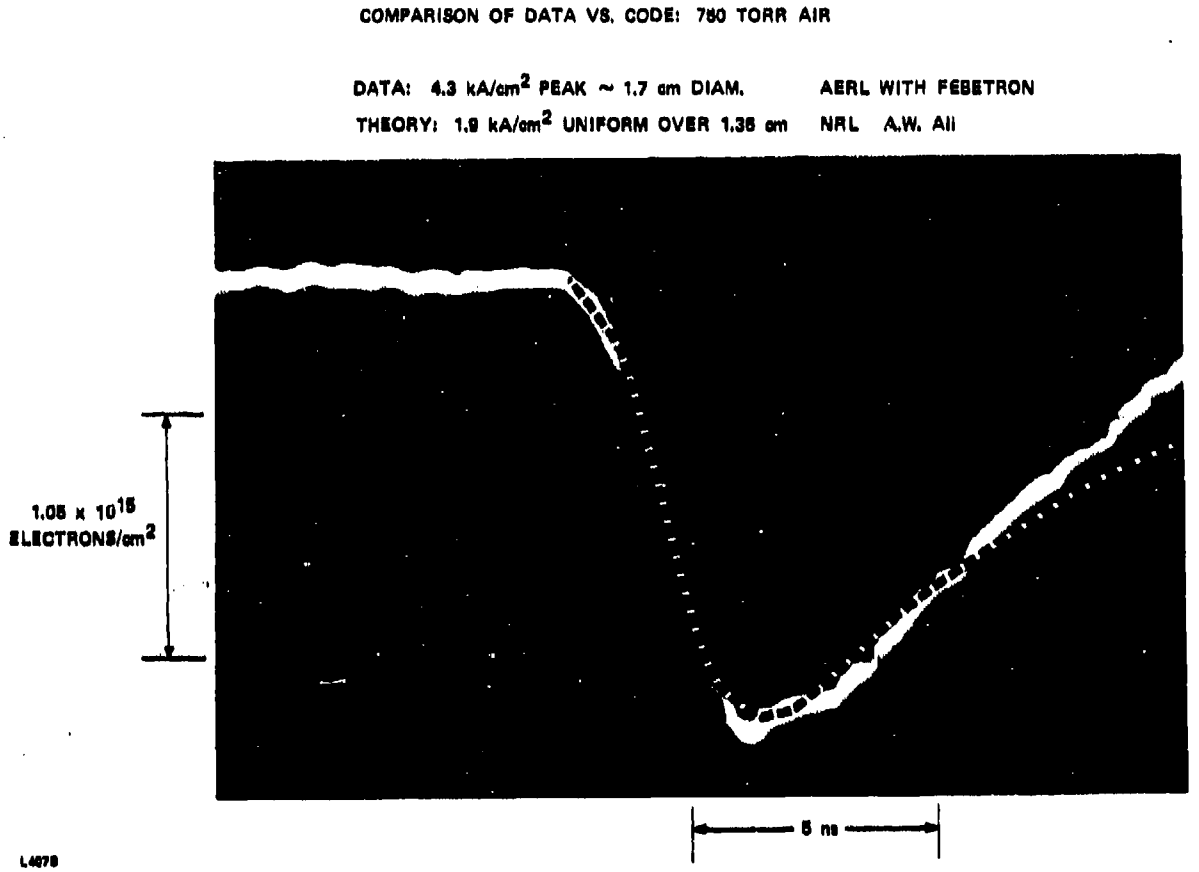

Figure 14. Comparison data vs code. Line integrated electron density in 760 torr air produced by Febetron pulse. Oscilloscope trace: produced by 4.3 kA/cm^2 peak axial current density with nominal 1.7 cm diam beam. Dashed curved: (A.W. Ali NRL) For 1.9 kA/cm^2 current density assuming distribution is uniform over 1.4 cm diameter.

During the decay portion of the curve, theory and data begin to diverge after about 5 ns. This difference is probably due to build up of metastable population during the recombination phase rather than due to an error in the theoretical recombination coefficients.

5.1.3 Nitrogen Data

Results of experiments performed with a nitrogen at 760 torr are shown in Figure 15. In the top trace, (a), the double pulse behavior is again seen followed by the calibration pulse. The base line slope of this trace is due to the feedback control. This occurs on a statistical basis when the e-beam happens to fire at the same time when the controller is making a step change in the voltage to the modulator. In the following trace, (b), the Marx voltage has been increased to 29 kV from the 28 kV used in trace (a). The double pulse behavior is eliminated with little modification to the first pulse. Careful inspection of the trace near the peak of electron density in (b) will show some evidence of noise getting into the horizontal oscilloscope sweep. The trigger cable, which derives its signal from a capacitive pickoff on the Febetron, is the most likely source for conducting the noise into the shielded room. The last trace, (c), was made with the reference beam blocked. A small amount of noise, on the order of a few percent of the peak electron signal, is evident over the period that the e-beam is firing.

The electron density scale in these shots corresponds to 7.5×10^{14} (electrons/cm^2)/division. Peak electron densities, essentially the same as for air at atmospheric pressure, of 1.8×10^{15} electrons/cm^2 are observed.

5.1.4 Argon Data

Figure 16 shows the result of data taken with argon gas at atmospheric pressure. Trace (a), which is taken at the same sensitivity as the nitrogen data, or 7.5×10^{14}/cm^2/div shows a rapid onset of electron density. The next trace, (b), is taken at a factor of ten less sensitivity, or 7.5×10^{15}/cm^2. Peak electron densities of 1.3×10^{16} are reached. For all practical purposes the response is still linear at this density.

NITROGEN 760 TORR

$n\ell$ = 7.5 x 10^{14} (ELECTRONS/cm^2) /div

A) 28 kV

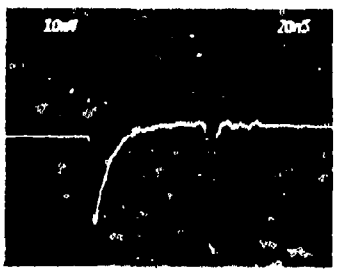

B) 29 kV

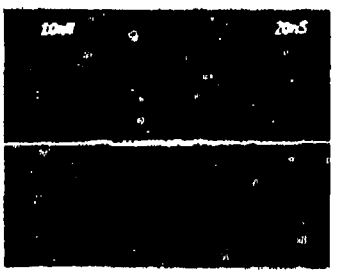

C) REFERENCE BEAM BLOCKED

L4090

Figure 15. Line integrated electron density produced in nitrogen at 760 torr by Febetron pulse. System sensitivity 7.5 x 10^{14} (electrons/cm^2)/division. (a) Marx bank charged to 28 kV. Results of Febetron double pulse evident, third pulse is calibration signal. (b) Marx bank charged to 28 kV. (c) Same as (b) but with reference beam blocked.

ARGON 760 TORR, 28 kV

$n\ell$ = 7.5 x 10^{13} (ELECTRONS/cm^2) PER mV

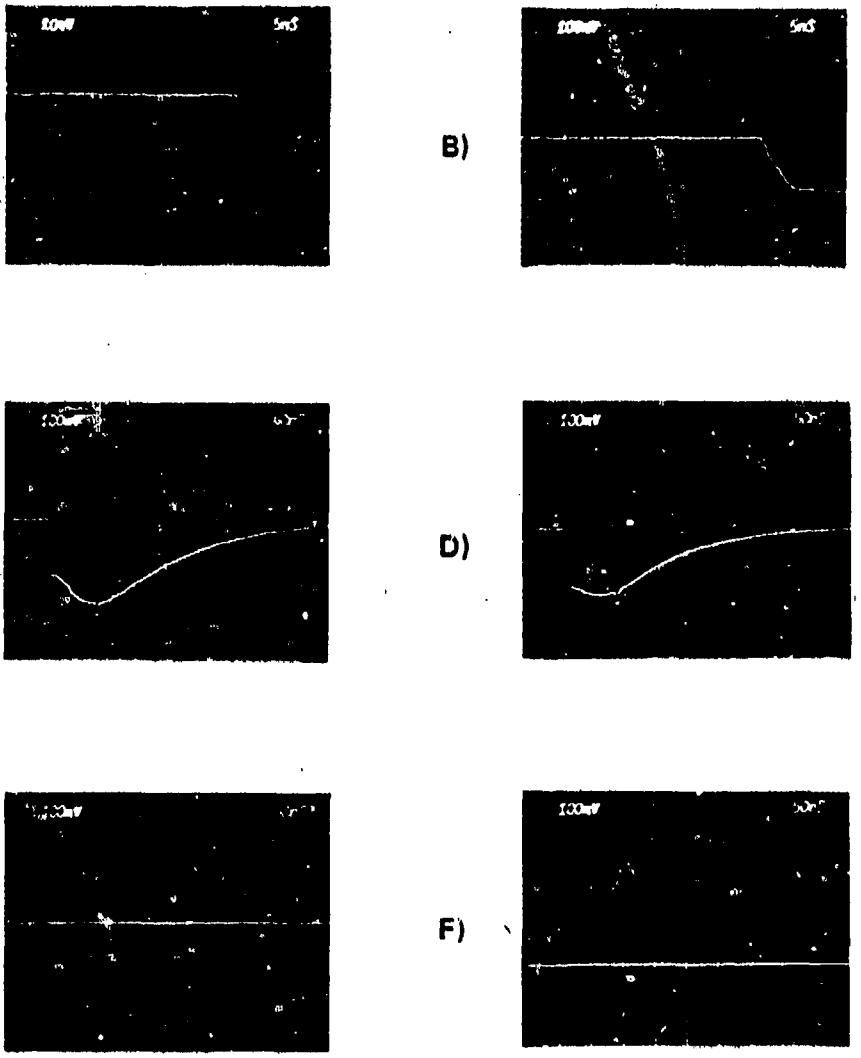

Figure 16. Line integrated electron density in argon at 760 torr with 28 kV Febetron charge. Vertical scale 7.5 x 10^{13} (electrons/cm^2)/mV. Traces (a)-(d) data from shots at varying sweep speed and sensitivities. (e) shot with scene beam only. (f) shot with scene beam only and negative channel only.

The next two traces, (c) and (d), are taken at a slower sweep speed. Differences between the two traces are representative of shot to shot variations. It will be noted that after the fast initial rise there is an apparent further increase in electron density which occurs on a 50 to 100 ns time scale. This effect could be, as in the air and nitrogen case, due to build up of metastable population levels with transitions near enough to the probe laser frequency so as to change the index refraction. Another interesting possibility is that the changes are indeed due to late ionization phenomena. A candidate process would be Penning ionization of one metastable level through collisions with another metastable atom. The blip seen on both traces at about 140 ns time is due to the calibration pulse applied to the fast modulator. Measurement of the amplitude of that blip verifies that the system sensitivity is not changed, even in the presence of the high electron densities that are encountered here.

Trace (e) shows the result of the usual protocol of checking the system response with the reference beam blocked. As with the other gases, there is no evidence of signal components from sources other than phase shifts. The last trace, (f), is taken with the reference beam blocked and with the positive channel of the detector bridge blocked. Hence the trace shows the result of a beam passing through the e-beam region and falling on a single detector. At time 60 ns there is a barely discernable wiggle in the trace, which could correspond to the onset of absorption or beam steering. An upper limit of a few percent can be put on its magnitude. At 140 ns time a remnant of the calibration pulse can be seen. This small signal is probably due to a slight misalignment of the modulator crystal which would result in a rotation of the polarization of the laser output, and subsequent rejection of part of the scene beam as the light hits the polarizing beam splitter crystal on the strongback.

5.2 ETA EXPERIMENTS

Experiments were conducted on the the ETA accelerator over a two-day period, April 5 and 6, 1984. Given the time available, the experimental objectives were limited to: A) testing the limits of the interferometer system, B) conducting a broad survey of the ionization produced as a function of pressure, C) to examine the response of different gases, specifically air and neon.

5.2.1 EMP Noise and System Sensitivity

Before committing the ETA time to the conduct of experiments with the interferometer, tests were done to measure the EMP picked up by the system instrumentation. Data was collected while the ETA was devoted to FEL experiments. An e-beam transport tube blocked the scene beam. In order to do the experiments under as realistic conditions as possible under that circumstance, the polarization of the beam leaving the screen room was adjusted such that all of the light energy passed through the reference leg of the interferometer.

The tests were conducted with the 7 x preamplifier on the output of the photodetectors, which is the maximum sensitivity configuration. In Figure 17a, an EMP resulting from the firing of the ETA can be seen when the door to the screen room was open. However, as is evident from trace (b), when the screen room door is closed, no EMP from the accelerator is discernable. This demonstrates the achievement of one of the primary design objectives.

System sensitivity was determined in the same manner here as at AERL; namely, a hot air gun was used to introduce turbulence in the scene beam, and the peak to peak excursion of the system output was observed. On the first day of the experiments, a value of V_p = 320 mV was obtained under the conditions of optimum tuning. On the following day, the figure was V_p = 460 mV

Because of the power limitations resulting from the laser damage, the system could not be run in the constant output power mode. Consequently, the laser power fluctuated during the experiments. Fortunately, the presence of the calibration pulse on each of the traces allowed for accurate determination of systems calibration under these circumstances.

An examination of traces in Figure 18 taken with air, show a system sensitivity ranging between 1.9 and 2.8 x 10^{14}/cm^2/division. On these same traces, a high frequency noise with peak to peak amplitude on the order of 0.2 divisions or less can be seen. The RMS value of this noise is on the order of 0.07 divisions or less. This may be translated into an equivalent RMS noise in the line integrated electron density of < 1.3 x 10^{13} electrons/cm^2. This comes close to our objective of being able to resolve 10^{14}/cm^2 with the signal to noise ratio of 10.

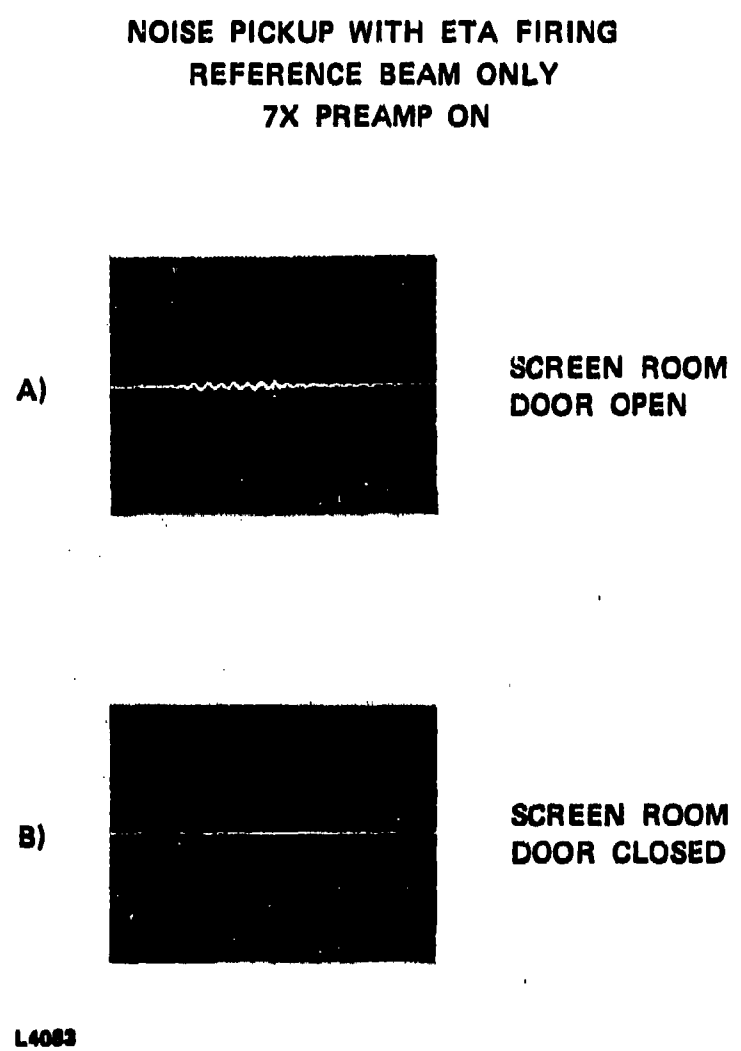

Figure 17. Noise pickup with ETA firing. Reference beam only, 7X preamp on. (a) Screen room door open. (b) Screen room door closed.

LINE INTEGRATED ELECTRON DENSITY IN AIR, 8 kamp ETA

$1.9 - 2.8 \times 10^{14}/cm^2$ PER div

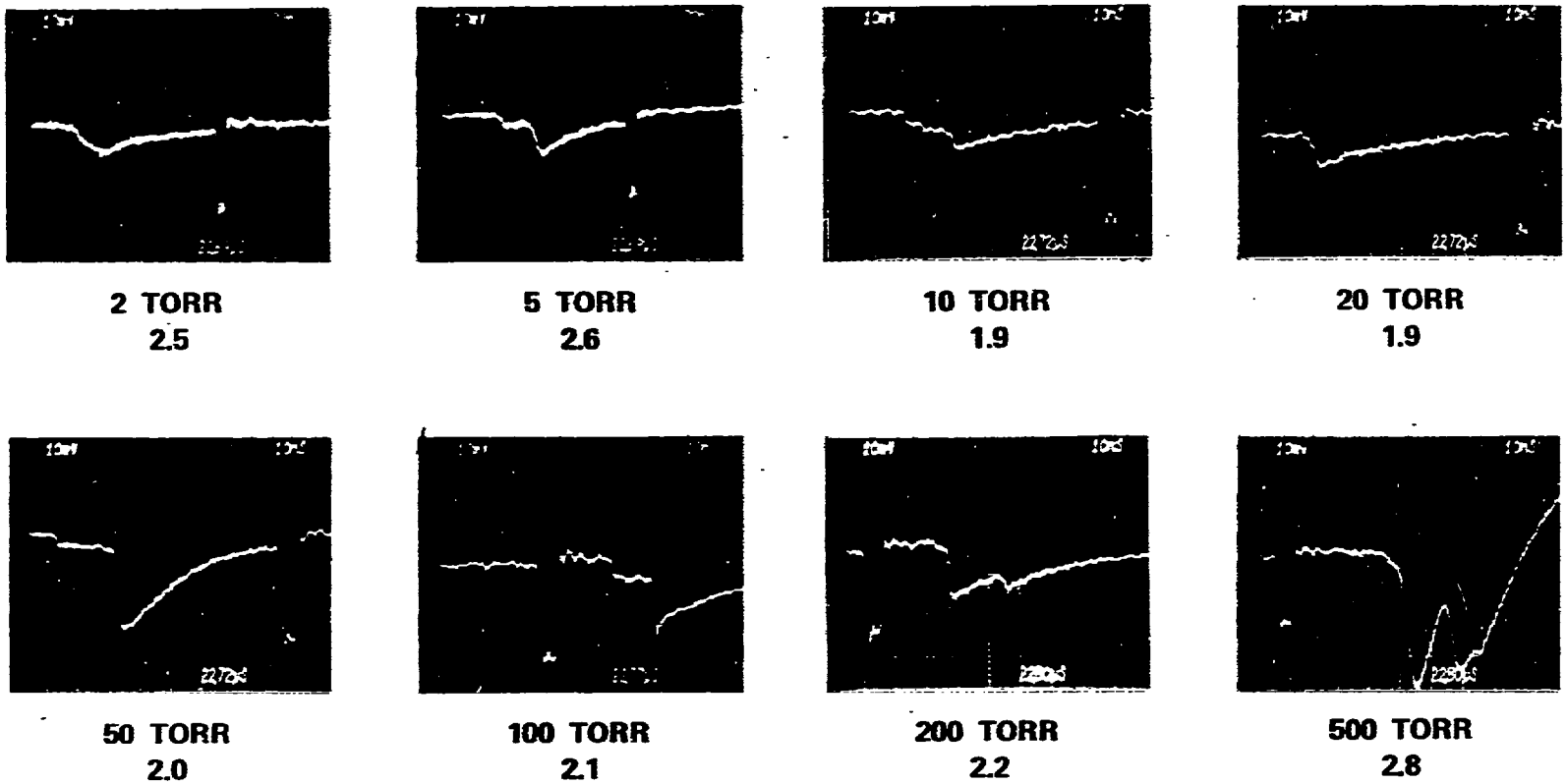

Figure 18. Line integrated electron density in air with 8 kA from ETA. 5 nsec pulse provides calibration. Sensitivity in units of $10^{14}/cm^2$/div and pressure appears below each trace.

Referred to the input of the preamplifier, the RMS noise level is < 100 μV. The preamplifier has a specified 7 db noise figure, which corresponds to a RMS noise of about 63 μV RMS. It appears that improvements beyond the original goals in the overall system sensitivity could be achieved by using state-of-the-art cooled preamplifiers and/or increased laser power.

At periodic intervals during the course of data taken, the remotely operated shutter for blocking the reference beam would be activated. Traces of the signal with the scene beam only were then recorded. Figure 19 trace (a) shows results obtained with the preamp in operation and 50 torr of air in the test cell. The displayed results should be compared with typical data, such as seen in Figure 18, with the reference beam unblocked. Figure 19 trace (b) shows the corresponding result with 500 torr in the test cell and no preamplifier. This can be compared with the signal obtained in Figure 23. The general conclusion is that all of the signal recorded is due to index of refraction effects, as opposed to noise pickup or intensity change.

5.2.2 Air Data

Artificial air consisting of 20 percent O_2 and 80 percent N_2 was employed. During a test sequence, the pressure in the experimental chamber would be set, and a number of traces, typically four, recorded on the scope. The pressure was then advanced to a higher value, usually following 2, 5, 10 sequence.

The scene beam was fixed in a vertical direction at the expected center of the e-beam. Because of previous damage to stepping motor drives, remotely driven vertical scans were not possible. Manual scans would have been too time consuming.

Figure 18 shows a collection of traces taken at different pressures. The beam exhibited considerable instability. Hence, shot to shot reproducibility was not to be had. Traces were selected for the presentation in this figure on the basis of being "typical".

A calibration pulse appears on each of the traces. Note that at pressures below 100 torr, the calibration pulse is always after the arrival of the e-beam front, while at 100 torr and above, the pulse was positioned before the

NO DETECTABLE SIGNAL WITH
REFERENCE BEAM BLOCKED
ETA @ 8 kamp

A)

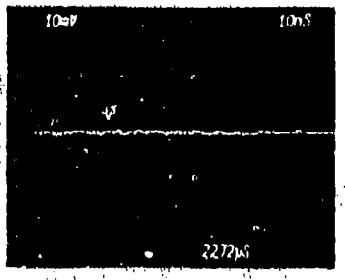

50 TORR AIR
7X PREAMP

B)

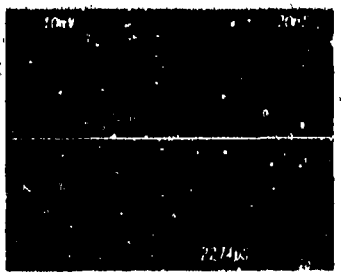

500 TORR AIR
NO PREAMP

L4084

Figure 19. Signals at maximum scope sensitivity with scene beam only and 8 kA from ETA. (a) 50 torr air, 7X preamp. (b) 500 torr air, no preamp.

arrival of the e-beam. On the basis of the calibration pulses, below each trace the sensitivity in units of 10^{14}/cm^2/major division is given.

Several general conclusions can be drawn from examination of the figures. First of the all, the total ionization produced does not depend very strongly on pressure. An overall view of pressure dependence is obtained from Figure 20 which plots the peak line integrated electron density measured on each of the shots on this run (these are designated x's on the figure). Only between 200 and 500 torr does there appear to be a major change in the amount of ionization produced.

At a pressure of 2 torr, only a single peak of ionization was observed. At the higher pressures, double humps of ionization were most often the rule. The time delay between the two events of increasing ionization was typically 15 -20 nsec. This is in comparison to an e-beam pulse width on the order of 25 nsec full width half max (See Figure 21a). The beam was undoubtedly thrashing around, as is evident from the beam bug traces of Figure 21. A general comparison of beam bug traces within the gas and the shape of the electron density profiles show a similar decay time. On the other hand, the rise time of electron density, as recorded by the interferometer, is considerably shorter than the net current rise time recorded on most beam bug traces. This may possibly be due to convective transport of a kink in the e-beam across the scene beam.

An attempt was made to correlate interferometer and beam bug traces from a given shot. This was difficult to do because the accelerator was firing at a 1 pps rate. Communications between the screen room and the accelerator control room were carried out on an intercom (with the screen room door partially open). It was not possible to assure that the traces corresponding to the same shot were pulled at both locations. However, Figure 22 shows the result of such an attempt. On the left-hand side of that figure, the line integrated electron density is presented, and on the right-hand side, the trace of the corresponding beam bug signal taken at a station immediately downstream from the interferometer scene beam crossing.

Figure 22a shows a sharp second rise in electron density. The downstream beam bug has a very sharp dip. In trace (b), the electron density only shows a single rise and the corresponding downstream beam bug trace has only a shallow dip.

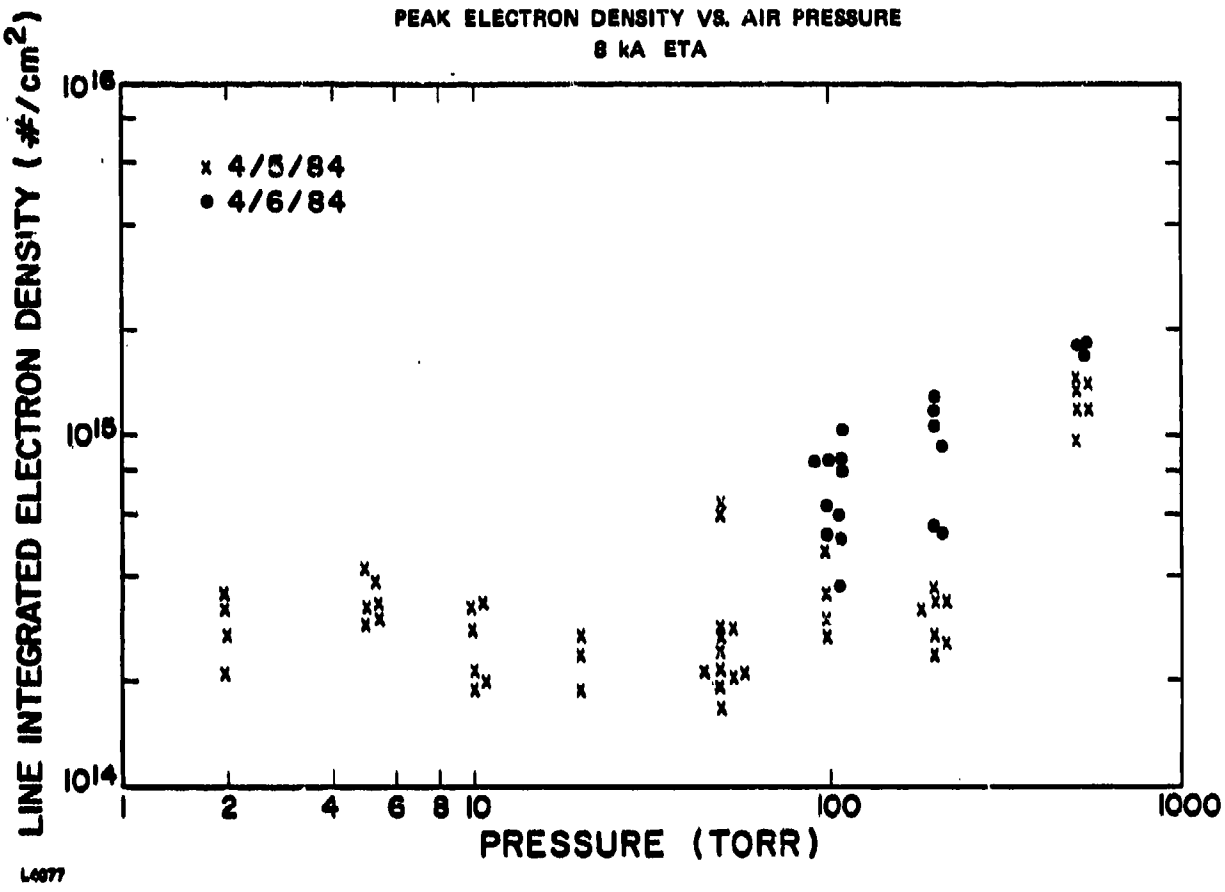

Figure 20. Peak line integrated electron density versus air pressure using ETA at 8 kA. X's from 4/5/84 data; solid dots from 4/6/84 data.

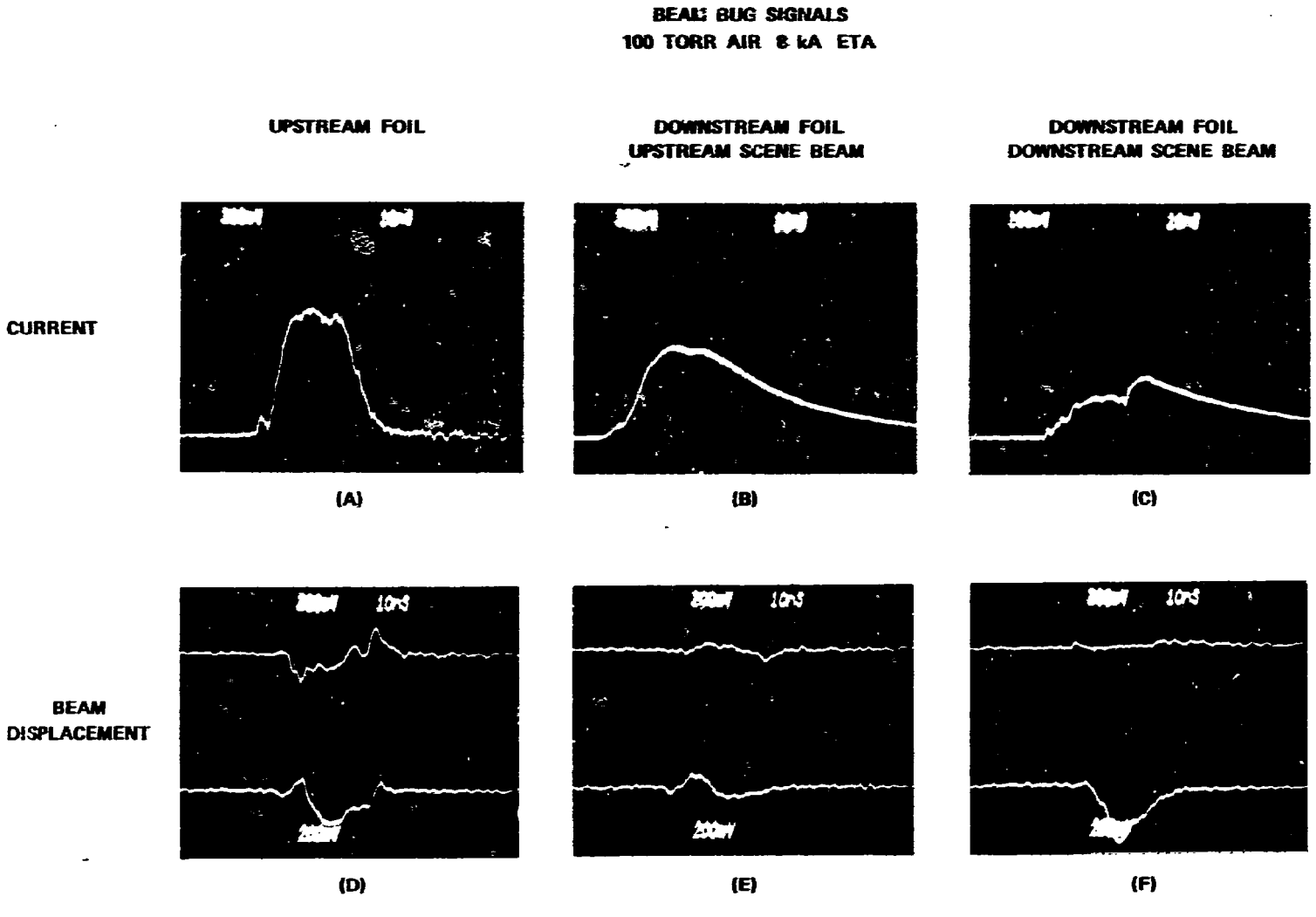

Figure 21. Beam bug signal from ETA at 8 kA with 100 torr air. Top traces, current beam bugs. Bottom traces, corresponding beam displacement bugs.

CORRELATION BETWEEN INTERFEROMETER AND BEAM BUG 50 TORR AIR @ 8 kA

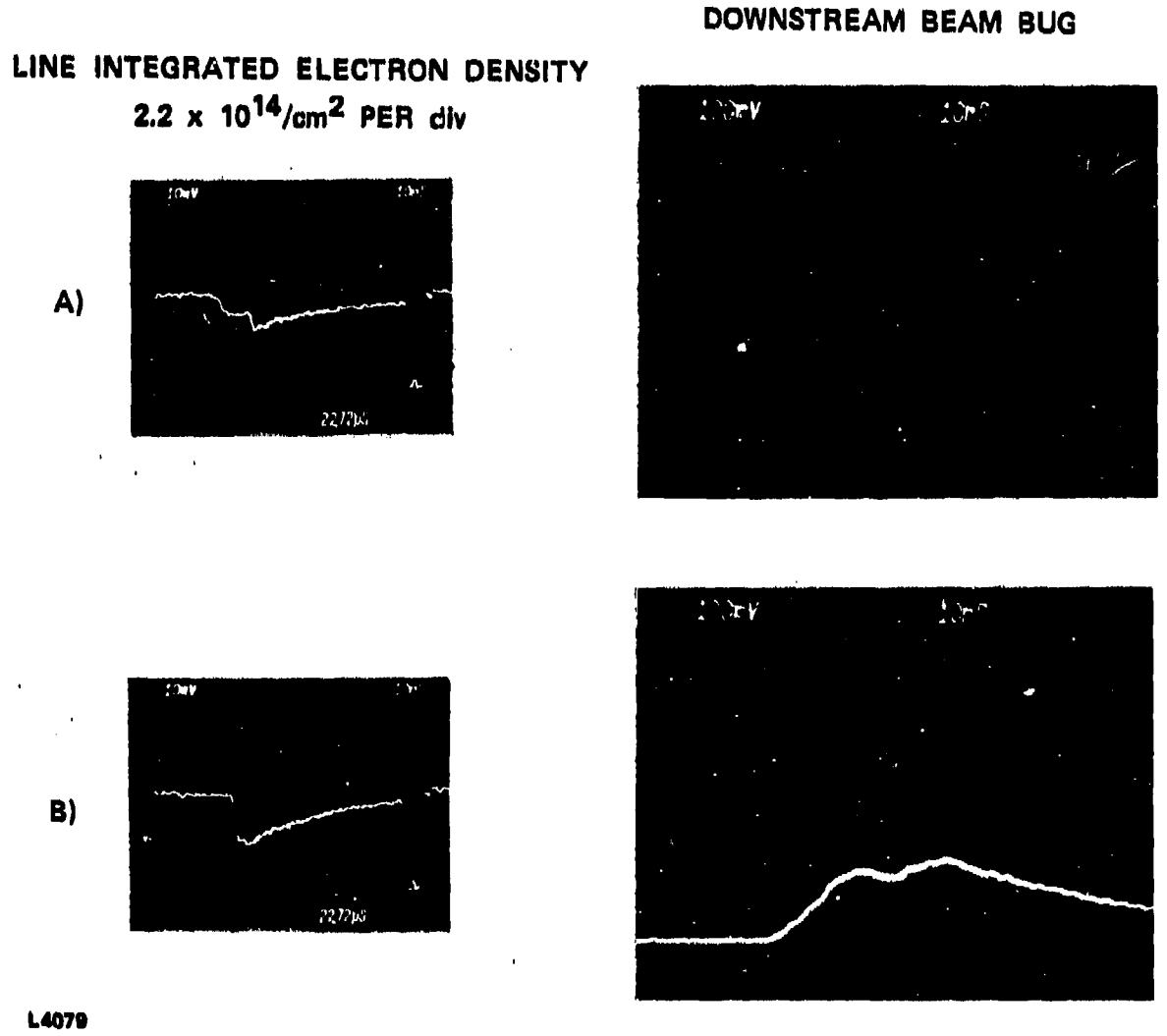

Figure 22. Correlation between interferometer and beam bug data. 50 torr air at 8 kA on ETA. Left-hand traces: line integrated electron density. Right-hand traces: corresponding downstream current beam bug signal.

It is clear that an important requirement for future experiments will be a good system for correlating beam bug data with the electron density measurements. It would be interesting, for instance, to know if the foot before the sharp rise observed in the traces at 200 torr and 500 torr (this was also observed in other shots at other pressures) corresponds to the prepulse seen in the trace (a) of Figure 21.

Additional data on air was taken during the second day of operation. In general, the beam behavior appeared to be more stable, with few traces exhibiting the double humped behavior observed on the day before. Figure 23 shows traces obtained on the two different days at a pressure of 500 torr.

The results of the peak electron density observed on the second day are also recorded in Figure 20. These shots are denoted by the solid circles. The electron densities are greater by a factor of roughly two.

An attempt was made during these runs to obtain a beam profile by scanning the magnetic field from one of the coils in the accelerator. Notice of changes in the coil settings would be relayed to the interferometer screen room over the intercom, and observations of increase or decrease in observed ionization behavior were fed back. Across the full range of adjustment the observed difference in electron density was not marked. The qualitative conclusion gained from this attempt is that the e-beam was quite broad.

During the next set of tests, which will take place on the ATA, the remote scanning capability of the interferometer will be available and should allow determination of the actual beam profile.

5.2.3 Neon Data

Experiments were conducted using neon gas over a pressure range from 20 to 500 torr. The e-beam on this day was relatively stable and, as with the second air run, presumed to be fairly large diameter.

Figure 24 shows the line integrated electron density over the range of pressures. These traces were selected on the basis of giving the largest deflection at a given pressure.

At 100 torr, three traces from three successive shots are presented. This serves to give an idea of the reproducibility of the data (the shift in the baseline from one shot to the other results from the finite accuracy of the automatic feedback control amplifier).

INCREASED BEAM STABILITY ON

SECOND DAY

500 TORR AIR – 1.4 x 10^{16} ELEC./cm^2 PER div

A)  4/5/84

B)  4/6/84

L4088

Figure 23. Comparison of line integrated electron density on two subsequent days. 500 torr air 1.4 x 10^{15}/cm^2/div on ETA. (a) 4/5/84. (b) 4/6/84.

LINE INTEGRATED ELECTRON DENSITY
NEON 8 kA ETA
1.5 – 1.8 x $10^{15}/cm^2$ PER div

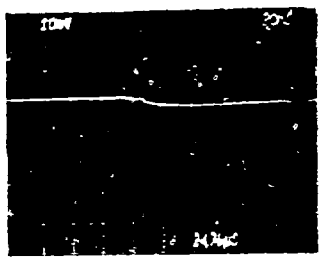

20 TORR

50 TORR

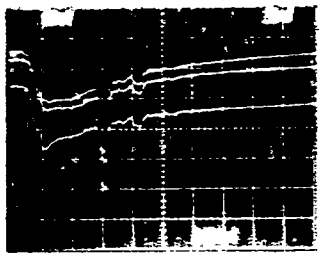

100 TORR

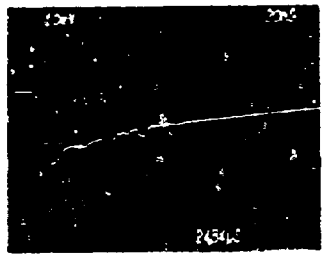

200 TORR

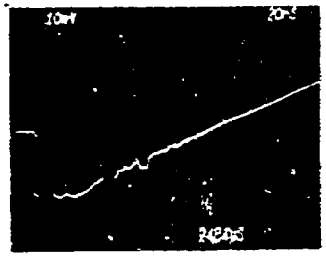

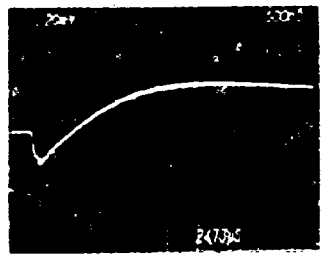

500 TORR

L4080

Figure 24. Line integrated electron density in neon. 8 kA from ETA. Pressure and sensitivity in units of $10^{15}/cm^2$/div below each trace.

The bottom traces, at 500 torr pressure, were taken from left to right at decreasing sweep speeds. At the 5 nsec/divisions sweep speed, a comparison of the risetime of the calibration pulse with the risetime of any of the features of the e-beam generated signal shows that all the features are temporally resolved. At the slowest sweep speed, 100 nsec/division, a large signal of opposite polarity to that produced by free electrons is observed. As discussed previously, this is presumably due to the generation of metastable states with large index of refraction.

The data of all the neon shots are plotted in Figure 25 as peak line integrated electron density versus pressure. From the very limited data available, one could argue proportionality between 2 and 100 torr and an onset of saturation at 100 torr.

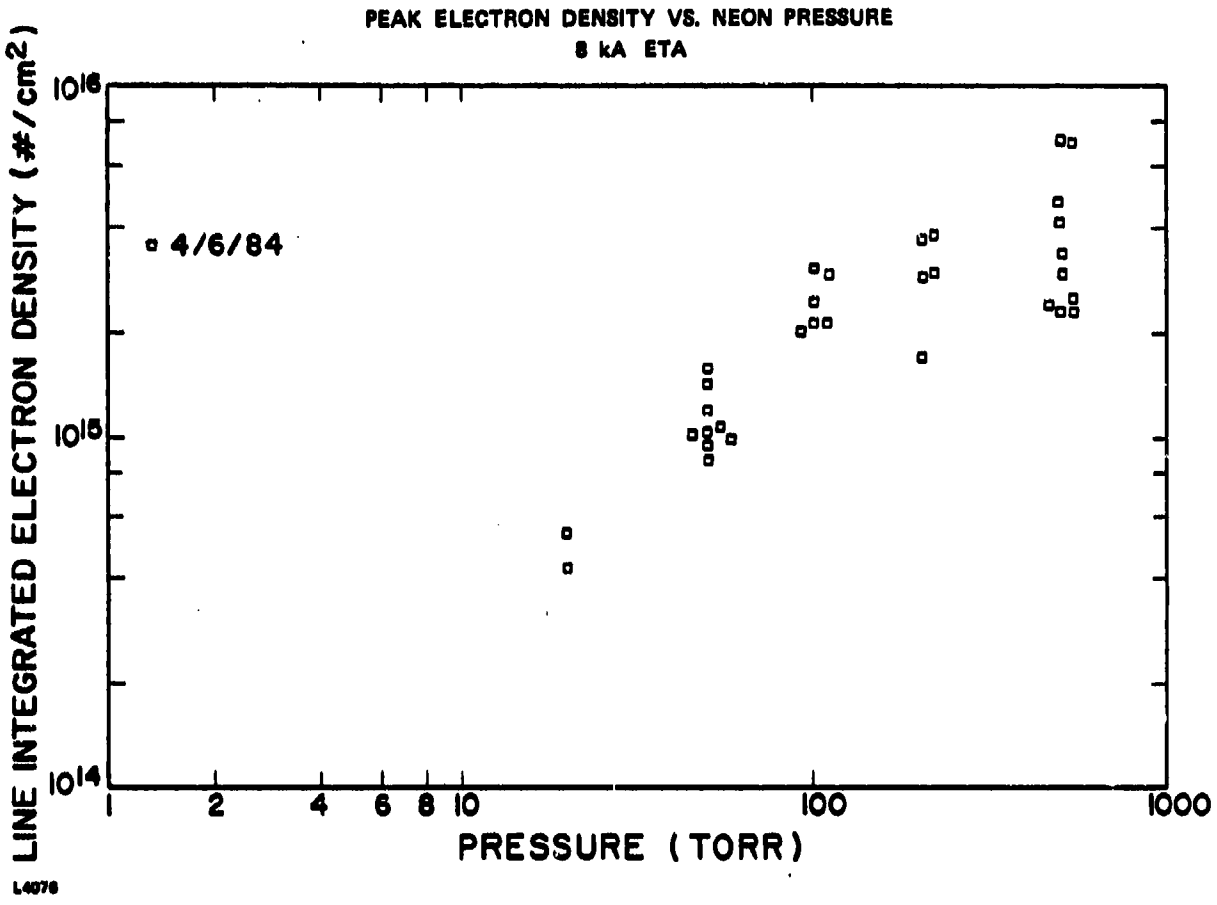

Figure 25. Peak line integrated electron density versus pressure in neon with 8 kA from ETA.

6.0 REFERENCES

1. Eckstrom, D.J. and Dickenson, J.S., "Diagnostic Development for E-Beam Excited Air Channels," SRI Tech. Rpt., Cont. No. N0000-14-81-C-0208, Feb. 1982.

2. Spitzer, Lyman, Physics of Fully Ionized Gases, Interscience, NY. p. 53.

APPENDIX A

INTERFEROMETER SIGNAL ANALYSIS

The laser beam exiting the interferometer strongback is composed of two mutually orthogonal polarization components. The first component, with a waveform designated by ψ_S ("S" for scene), has had its phase, ϕ_S, modified by the e-beam generated electron density. Its amplitude, A_S, might also have been modified by absorption processes in the e-beam interaction region. The second polarization component, designated by ψ_R, ("R" for reference), has an amplitude A_R and a phase ϕ_R. This wave follows the reference beam path of the interferometer.

$$\psi_S = A_S \cos(\omega t - \phi_S) \qquad \text{(A-1)}$$

$$\psi_R = A_R \cos(\omega t - \phi_R) \qquad \text{(A-2)}$$

On returning to the screen room, the two waves may no longer be linearly polarized due to reflection from mirrors orientated such that the polarization vectors are neither in, nor perpendicular to, the plane of incidence. Indeed, this is the case for mirror setups used with the Febetron and on ETA. However, measurements have put the degree of departure from linear polarization as small, < 10 percent. Hence, this effect will be neglected in the following analysis.

Even in applications in which the mirrors introduce a large degree of elliptical polarizations, it is our tentative understanding that the end result of the analysis would not be changed. This is because, with lossless dielectric mirrors, it is expected that the generally elliptic scene and reference beams will remain orthogonal to each other in the sense that the time averaged projection of one E field on the other is zero.

Upon entering the shielded room, the beam falls on a polarizing beam splitting cube which serves to mix the scene and reference beam fields. This cube separates the beam into two separate linearly polarized beams, ψ_1 and ψ_2, which exit the cube at right angles to each other. The waveforms ψ_1 and ψ_2 are each a linear combination of the waveforms ψ_S and ψ_R (Eq. (A-3) and (A-4)).

$$\psi_1 = \psi_S \cos\alpha - \psi_R \sin\alpha \qquad \text{(A-3)}$$

$$\psi_2 = \psi_S \sin\alpha + \psi_R \cos\alpha \qquad \text{(A-4)}$$

In these expressions, α represents the angle between the polarization vector of ψ_S and the polarization axis of the cube. Usually α is adjusted by means of a halfwave plate such that ψ_1 and ψ_2 are each composed of equal parts of ψ_S and ψ_R. To meet this condition, α is 45°. In general there will be some error in the alignment, designated by Δ, and α is given by Eq. (A-5).

$$\alpha = \pi/4 + \Delta \qquad \text{(A-5)}$$

The instantaneous time dependent waveforms are not of particular interest. Rather, the photodetectors respond to the time average of the square of the waveforms. Equations (A-6) and (A-7) give the results of squaring Eqs. (A-3) and (A-4) and taking the time average.

$$\langle \psi_1^2 \rangle = \frac{A_S^2}{2}\,\frac{1-\sin 2\Delta}{2} + \frac{A_R^2}{2}\,\frac{1+\sin 2\Delta}{2} - \frac{A_S A_R}{2}\cos 2\Delta \sin\delta\phi \qquad \text{(A-6)}$$

$$\langle \psi_2^2 \rangle = \frac{A_S^2}{2}\,\frac{1+\sin 2\Delta}{2} + \frac{A_R^2}{2}\,\frac{1-\sin 2\Delta}{2} + \frac{A_S A_R}{2}\cos 2\Delta \sin\delta\phi \qquad \text{(A-7)}$$

In these expressions the substitution

$$\phi_S - \phi_R = \delta\phi - \pi/2 \qquad \text{(A-8)}$$

has been made.

The automatic feedback circuit attempts to continually maintain the phase difference between the scene beam and the reference beam at $\pi/2$, even in the presence of vibrations and of turbulence in the e-beam interaction area. When the high powered e-beam generates electron density in the background gas, a phase shift $\delta\phi$ arises. The nanosecond time scale of this event is far too fast for the active circuitry to follow.

The waves $_1$ and $_2$ fall on two individual pin diode detectors. The resulting current responses are given by Eqs. (A-9) and (A-10).

$$I_1 = Q_1 \langle \psi_1^2 \rangle \qquad \text{(A-9)}$$

$$I_2 = Q_2 \langle \psi_2^2 \rangle \qquad \text{(A-10)}$$

Here the factors Q_1 and Q_2 represent the total effects of collection efficiency, attenuation, and quantum efficiency of the detectors.

Examinations of Eqs. (A-6) and (A-7) show that it is the third term in each which represents the useful signal due to the presence of the factor $\sin\delta\phi$. (For all present applications $\sin\delta\phi$ is approximately equal to $\delta\phi$.) If either signal strength, A_S or A_R, changed on a time scale comparable to the fast time scale of $\delta\phi$, this would represent a competing source of noise. Numerous mechanisms could cause changes in A_S and/or A_R. The laser intensity could change, which would change both A_S and A_R by the same factor. The polarization vector of the laser could wander. This would cause A_S to change in the opposite direction to that of A_R. The scene beam could be partly absorbed by atomic species in the e-beam interaction region. This possibility was investigated at SRI.[1] A consequence of such absorption would be a decrease in A_S alone.

Changes in wave amplitude, either of A_S or A_R will be designated as δA, and for algebraic simplicity the distinction between A_S and A_R will be dropped. It will be assumed that the polarizing cube is adjusted so that the angle Δ is equal to zero. Then examination of Eqs. (A-6) or (A-7) gives the signal, S_1, to noise, N_1 ($\propto A\delta A$), ratio expected if either of the two beams is monitored.

$$\left| \frac{S_1}{N_1} \right| \simeq \left| \frac{\delta\phi}{\delta A/A} \right| \qquad \text{(A-11)}$$

This equation is modified by a factor of two dependent on whether A_S, A_R or both, have time varying components.

The interferometer is designed to have a sensitivity on the order of 10^{14} electrons/square centimeter. This corresponds to a $\delta\phi$ of about 2×10^{-3}. If the signal to noise ratio is to be unity or greater, then $\delta A/A$ must be less than or equal to about one part per thousand (likewise for the variation in intensity, within a factor of two).

The laser for this program was especially selected on the basis of its low noise characteristics in the region extending from 50 MHz to beyond 1 GHz. Measurements showed that the noise was less than one part per thousand. The SRI experiments[1] indicated that absorption of the scene beam in the e-beam generated plasma could be on the order of a few parts per thousand when $\delta\phi$ was still near the limits of resolution. Consequently, during the low electron density portions of the measurements, a signal to noise ratio on the order of unity can be expected if only one of the analyzed beams is monitored.

A substantial improvement in the signal to noise ratio may be achieved if the two analyzed signals are both monitored through their difference. In practice, the currents are subtracted in a high speed bridge circuit.

$$I_\Delta = I_2 - I_1 \qquad \text{(A-12)}$$

$$= (Q_2 - Q_1)\ \frac{A_S^2+A_R^2}{4} + (Q_1+Q_2)\sin 2\Delta\ \frac{A_S^2-A_R^2}{4}$$
$$+ (Q_1+Q_2)\ \cos 2\Delta\ \frac{A_S A_R}{2}\ \sin\delta\phi \qquad \text{(A-13)}$$

Since we have arbitrarily chosen the subscript 1 to designate the current that is subtracted, contributing a negative component to the signal on the scope, that signal will heretofore be referred to as the negative channel. Correspondingly, the subscript 2 will be designated the positive channel.

The difference signal is composed of three terms, the first two of which depend on the wave amplitudes and not the phase. Hence, they are a potential source of noise. The last term is proportional to the signal. The first term can be made very small by adjustment of Q_1 or Q_2 using a variable attenuator in front of one of the detectors. The second term is made small by rotating the polarization so that $\Delta \approx 0$ using a half wave plate upstream of the mixing element and/or by making $A_S^2 \approx A_R^2$ through adjustment of angle at polarization before the beam leaves the screen room.

The last term, which determines the sensitivity of the system, is maximized by having the angle Δ equal to zero, and A_S equal to A_R. For convenience we make the substitution in the last term.

$$(Q_1 + Q_2)\ \cos\ 2\Delta\ \frac{A_S A_R}{2} = \frac{V_P}{R} \qquad \text{(A-14)}$$

Here R is the circuit impedance, normally 50 Ω. then the variable part of the voltage signal will be

$$V = V_p \sin\ \delta\phi \qquad \text{(A-15)}$$

The parameter V_p may be determined experimentally simply by forcing the system through a phase change of $|\delta\phi| \geq \pi$, and observing the maximum voltage obtained.

Returning to the question of signal to noise under the same simplifying assumptions as before, the signal to noise ratio can now be written,

$$\left|\frac{S_\Delta}{N_\Delta}\right| \approx \left|\frac{\delta Q}{2Q} + \delta\phi\right|^{-1} \frac{\delta\phi}{\delta A/A} \qquad \text{(A-16)}$$

where $Q = (Q_1+Q_2)/2$ and $\delta Q = Q_2-Q_1$.

It is seen that if the two channels are balanced so that the fractional error in the sensitivities is on the same order as $\delta\phi$ or no worse than a few parts per thousand, then the signal to noise ratio becomes

$$\left|\frac{S_\Delta}{N_\Delta}\right| \approx \left|\frac{A}{\delta A}\right| \quad \text{for } \frac{\delta Q}{Q} < \delta\phi \qquad \text{(A-17)}$$

As an example, a signal to noise ratio of 10 is achieved even in the presence of intensity variations as large as 5 percent, noting the relation

$$\left|\delta A/A\right| = \frac{1}{2}\left|\delta I/I\right| \qquad \text{(A-18)}$$

A considerably more conservative objective would be the achievement of a balance with

$$\left|\delta Q/Q\right| \leq 0.1 \gg \left|\delta\phi\right| \qquad \text{(A-19)}$$

This degree of balance is readily achievable in practice over extended periods without system adjustment. Then from Eq. (A-14)

$$\left|\frac{S_\Delta}{N_\Delta}\right| \approx 4\,\frac{|\delta\phi|}{|\delta Q/Q|\,|\delta I/I|} \quad \text{for } \frac{\delta Q}{Q} \gg \delta\phi \qquad \text{(A-20)}$$

This insures an overall signal to noise ratio of at least 10 at the design sensitivity of $\delta\phi = 2 \times 10^{-3}$ in the presence of the worst expected intensity variation of $\delta I/I \approx 3 \times 10^{-3}$.

APPENDIX B

PHASE SHIFT DUE TO ELECTRON DENSITY

The index of refraction experienced by a beam of light propagating through an unmagnetized plasma may be expressed in terms of the plasma frequency, ω_p, and the angular frequency of the light, ω (see Ref. 2).

$$\eta = \sqrt{1 - \frac{\omega_p^2}{\omega^2}} \tag{B-1}$$

where ω_p is

$$\omega_p^2 = \frac{4\pi n e^2}{m} \tag{B-2}$$

In this expression, n is the electron number density, and e and m represent the electron charge and mass, respectively.

For the electron density regime of interest and assuming an optical frequency, we have that ω is much greater than ω_p. Then the expression for the index may be simplified to

$$\eta - 1 \approx - \frac{n r_e \lambda^2}{2\pi} \tag{B-3}$$

Here λ is the wavelength of the light and r_e is the classical electron radius.

The net phase shift experience by the light beam is obtained from a line integral of the index over the light path.

$$\delta\phi = \frac{2\pi}{\lambda}\int d\ell\ (n - 1)$$
$$= - r_e \lambda n\ell \qquad \text{(B-4)}$$

In the second from of Eq. (B-4) we have written the integral of the electron density over the path as though the electron density were constant over a distance ℓ. In general, this will not be true and the product $n\ell$ should be understood as the integral of a variable electron density over the optical path.

The design goal of the interferometer is a measurement of $n\ell = 10^{14}$ electron/cm^2 with a signal to RMS noise ratio of 10. This corresponds to measuring a $\delta\phi$ of 2×10^{-3}, or $\lambda/3400$. The operating wavelength of the system 0.6471 μ has been used in the evaluation of Eq. (B-4).

In Appendix A it was shown how the voltage output signal of the interferometer was related to the phase shift (see Eq. (A-15)). If the phase shift is sufficiently small this expression may be written

$$\delta\phi \approx \frac{V}{V_p} \qquad \text{(B-5)}$$

Here V is the voltage corresponding to the phase shift $\delta\phi$, and V_p is the maximum voltage observed when the system has been forced thorugh a phase shift of at least π rad.

Substituting this expression for the phase shift into Eq. (B-4), obtain

$$n\ell \approx \frac{1}{r_e \lambda}\ \frac{V}{V_p}$$
$$= 5.5 \times 10^{16}\ \frac{V}{V_p}\ \text{electrons/cm}^2 \qquad \text{(B-6)}$$

DISTRIBUTION LIST

Director, Defense Advanced Research Projects Agency, 1400 Wilson Boulevard, Arlington, VA 22209	Attn: Dr. Joseph A. Mangano LTCOL Richard L. Gullickson
Office of Naval Research, 800 North Quincy Street, Arlington, VA 22218	Attn: Dr. Charles W. Roberson
Commander, Naval Sea Systems Command, PMS-405, Washington, DC 20362	Attn: Mr. David L. Merritt
Commanding Officer, Naval Research Laboratory, 4555 Overlook Avenue, SW, Washington, DC 20375	Attn: Dr. J. Robert Greig (4763) Dr. Martin Lampe (4763)
Naval Postgraduate School, Department of Physics (Code 61), Monterey, CA 93940	Attn: Professor Kai Woehler
U. S. Army Ballistic Research Laboratory, DRDAR-BLB, Aberdeen Proving Ground, MD 21005	Attn: Dr. Donald Eccleshall
Director, BMD, Advanced Technology Center, P.O. Box 1500, Huntsville, AL 35807	Attn: Mr. Milton C. Hawie (BMSATC-1)
AFOSR, Physical and Geophysical Sciences, Bolling Air Force Base, Washington, DC 20332	Attn: CAPT Henry L. Pugh, Jr.
Air Force Weapons Laboratory, Kirtland Air Force Base, Code NTY, Albuquerque, NM 87117	Attn: Dr. David C. Straw
Central Intelligence Agency, OSWR, P.O. Box 1925, Washington, DC 20013	Attn: Dr. Jose P. Pina
Department of Energy, Washington, DC 20545	Attn: Dr. James E. Leiss Mr. Gerald J. Peters Dr. Terry F. Godlove (G-246) Dr. Marshall Sluyter (DP-231)
Department of Commerce, National Bureau of Standards, Building 245, B-102, Washington, DC 20234	Attn: Dr. Samuel Penner Dr. Mark A. D. Wilson
Lawrence Livermore National Laboratory, Univ. of California, P.O. Box 808, Livermore, CA 94550	Attn: Dr. William A. Barletta (L321) Dr. Daniel S. Prono (L436)
Lawrence Berkeley Laboratory, 1 Cyclitron Road, Berkeley, CA 94720	Attn: Dr. Edward P. Lee Dr. Thomas J. Fessenden
Los Alamos National Laboratory, P.O. Box 1663, Los Alamos, NM 87545	Attn: Dr. Thomas P. Starke, P942
Oak Ridge National Laboratory, Health and Safety Research Director, Oak Ridge, TN 3780	Attn: Dr. Rufus H. Ritchie
The Charles Stark Draper Laboratory, 555 Technology Square, Cambridge, MA 02139	Attn: Mr. Edwin A. Olsson
Advanced Technology & Mission Analysis, Gould Inc., ASD, 1235 Jefferson David Hwy, Arlington, VA 22202	Attn: Dr. Henry Hidalgo
Directed Technologies, Inc., 1225 Potomac School Road, McLean, VA 22101	Attn: Dr. Ira F. Kuhn, Jr.
LaJolla Institute, P.O. Box 1434, La Jolla, CA 92038	Attn: Dr. Keith A. Brueckner
Lockheed Palo Alto Research Laboratory, 3251 Hanover Street Building 203, Dept. 52-11, Palo Alto, CA 94304	Attn: Dr. John G. Siambis
McDonnell-Douglas Research Laboratory, P.O. Box 516, St. Louis, MO 63166	Attn: Dr. J. Carl Leader
Mission Research Corporation, 1720 Randolph Road, SE, Albuquerque, NM 87106	Attn: Dr. Brendan B. Godfrey
Mission Research Corporation, P.O. Box 719, Santa Barbara, CA 93102	Attn: Dr. N. J. Carron
Pulse Sciences, Inc., 2001 Wilshire Boulevard, Suite 600, Santa Monica, CA 90403	Attn: Dr. John R. Bayless
Sandia National Laboratories, Division 1246, Albuquerque, NM 87185	Attn: Dr. R. Bruce Miller
Science Applications, Inc., 5150 El Camno Real, Suite B-31, Los Altos, CA 94022	Attn: Dr. Robert R. Johnston
SRI International, PS0015 Molecular Phsics Laboratory, 333 Ravenswood Avenue, Menlo Park, CA 94025	Attn: Dr. Donald J. Eckstrom
Defense Technical Information Center, Cameron Station, Alexandria, VA 22314	10 copies of unclassified final reports 3 copies if classified
Commander, Naval Surface Weapons Center, White Oaks, Silver Spring, MD 20910	Attn: Dr. C. M. Huddleston (R401) Dr. E. E. Nolting (F53) Dr. H. S. Uhm (R41) Dr. R. B. Fiorito (R41) Library (E43-Data Bank) 3 copies